4. FINAL REPORT

4.1 Final publishable summary report

4.1.1 Executive summary

The resistance at the metal contact-semiconductor interface and recombination at the passivating layer-semiconductor interface are two important bottlenecks for improving the performance of current solar cells. These processes are quantum mechanical by nature, but so far most studies and attempts to improve the properties of solar cells have been at the device scale. A main reason for this is the great challenges faced by theoretical modelling. Accurate descriptions of the geometric and electronic structures are required, which necessitate the use of highly sophisticated methodologies based on first principles. At the same time, the interfaces extend in many cases well beyond the size limit of first principles methods, creating the need for more efficient methods, which can operate at larger time and size scales. HiperSol aimed at filling this knowledge gap by developing and implementing a multi-scale modelling environment, focusing on real interfaces and how the achieved knowledge can be used to enhance the present solar cell technology. The physics at the various scales was treated by a multitude of techniques, and the boundaries between these techniques were of utmost importance for the success of the project. Hence, considerable emphasis was laid on consistently connecting different methods and on experimental validation.

For both the contacting and passivating interfaces realistic atomic configurations have been constructed based on relaxation using a combination of density functional theory and empirical molecular dynamics as well as experimental input from mainly advanced transmission electron microscopy. An important development has been the implementation of semi-empirical pseudo-potentials, which can calculate the accurate electronic structure of large structures with up to millions of non-equivalent atoms.

For the contacting interface these structures have been used to calculate the quantities relevant for modelling at larger scales, like diffusivities in melted glass and Schottky barriers at the silicon/metal contact interface. A phase field model has been constructed for predicting the metal transport through the melted glass during the firing process and compared with experiments, including a new technique combining selective etching with scanning electron microscopy. The contact resistivity has been modelled with finite elements for both flat and textured metal/silicon interfaces.

For the passivating interface different defects and traps have been classified based on theoretical and experimental investigations. Atomic interface structures with different defects/traps were used to construct envelope functions from which the life times were calculated. A novel method for obtaining Auger recombination rates directly from first principles has also been developed. It has also been shown how an interface gradient in nitrogen concentration can affect the quality of passivation and the anti-reflecting properties (through the refractive index). The width of the depletion layer affects the density and distribution of bond types and defect states known to be important for the performance of solar cells where amorphous SiN_x is used as an anti-reflective coating. Our results suggest that a graduated interface can be designed to improve the efficiency of solar cells.

The HiperSol project has resulted in several journal publications and education of students and research staff as well as improved industrial routes. A key factor for this success has been the close collaboration between academia, research and industry partners.

4.1.2 Project context and objectives

The HiperSol (Modelling of Interfaces for High Performance Solar Cell Materials) project was a small- and medium scale project within the EU 7th framework programme. The overall aim of the project was to develop an integrated multi-scale modelling environment that is applicable to properties of real materials on length scales not accessible by ab initio modelling; and to use this environment to accurately describe and predict important parameters and properties of interfaces of contacting and passivation layers with silicon, in order to enable a drastic decrease of the cost/efficiency ratio of a solar cell device. This three year project started on December 1st 2009 and had a total budget of 4.5 million Euro of which the funding from the European Commission was 3.4 million Euro.

Motivation for the HiperSol project

Improvements in the field of materials science and nanostructured materials in particular, increasingly require fundamental understanding of important aspects like interfaces, and thus modelling at many different scales. The industrial shift towards a knowledge-intensive economy demanded radical innovation in the design of new material systems for specific highly-demanding applications. This implies that designs based on phenomenological and macroscopic material property measurements no longer suffice for this increasing demand. Engineering tools, associated with multi-scale modelling and simulation approaches, can help by including the microscopic, or even more accurate atomistic, structure and properties into materials design, in order to construct more reliable high performance materials, based on an accurate prediction of their in-service behaviour.

Solar cells were chosen both because of their modelling challenges, and also because of their relevance for the development of sustainable energy resources in Europe as well as in the rest of the world. In many energy scenarios, solar electricity will dominate electricity production within the coming 50 years. For this to become true, the costs have to be decreased while simultaneously realising high efficiencies. This requires in-depth knowledge about the behaviour of the most crucial processes in solar cell devices, enabling the optimisation of solar cell design and solar cell processing. Despite the conceptual simplicity of today's solar cells, a detailed understanding is still lacking, in particular of many of the interface-related mechanisms. In order to achieve the necessary breakthroughs in solar cell manufacturing, fundamental understanding and accurate predictions are required and can only be achieved by advanced modelling including all the relevant scales.

Project scope

The HiperSol project focused on two interfaces, the contacting interface between silicon and the silver finger and the passivating interface between silicon and the passivating layer since the resistive and recombination losses at these interfaces are responsible for the major loss mechanisms for the light generated carriers (electrons and holes) in standard Si-based PV. These interfaces are schematically shown in Figure 1. Even though the modelling framework developed in HiperSol is specifically designed for contacting and passivation interfaces in solar cells, the generic character of the methodology spreads the impact other fields within materials science and engineering.

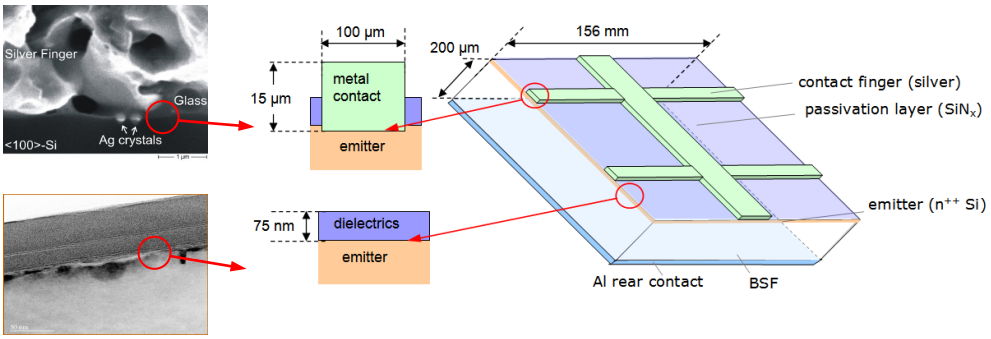

Figure 1. *Solar cell with the contact and passivation interfaces marked.*

HiperSol's objectives

The **first objective** of the HiperSol project was to develop general methodology and models on the atomistic level for theoretical studies of interfaces and other complex structures at the nano-scale.

To realise this it was necessary to develop a methodology capable of describing a macroscopic system, with properties determined on a quantum mechanical level. To create such a methodology, the following subgoals had to be met:

- Construction of inter-atomic potentials for empirical molecular dynamics (EMD) from first principles (FP) calculations.
- Determination of realistic and representative atomistic structure models as a basis for further ab initio calculations.
- Creation of semi-empirical pseudo-potentials (SEPP) based on first-principles calculations.
- Development of techniques for accurate calculation of electronic band structures in sub-systems large enough to include macroscopically relevant features.

In order to enhance the impact of this work, it was an important goal to make the solution generally applicable and accessible.

The **second objective** of HiperSol was to construct a validated multi-scale modelling environment specifically aimed at describing and predicting important properties of contact interfaces in silicon solar cells.

The integrated modelling environment for the contacting interface should provide realistic atomistic models of the dynamic metallization process as well as calculating conductivities of the static contacting interfaces from first principles with the following output:

- Diffusion parameters obtained from FP and EMD calculations.
- Surface and interface energies calculated from FP or EMD.
- Electric conductivities from FP calculations and Boltzmann theory.
- Detailed models of the metallization processes obtained with FEM simulations.
- Global conductance of a contacting finger from FEM simulations.

These results depend strongly on the development of a general methodology, and an essential goal was to successfully integrate the different length and time scales involved in the modelling approaches. Another essential goal was to obtain a systematic and reliable scheme for experimental validation of the theoretical tools.

The **third objective** of HiperSol was to create a validated and integrated multi-scale modelling environment for accurately calculating the most relevant properties of the passivation interface in silicon solar cells.

The integrated modelling environment for passivating interfaces should provide accurate band structure calculations and charge carrier recombination rates at the interface from first principles calculations. The expected output included the following:

- Electronic band structures of simple interfaces from FP calculations and of more complicated surfaces from SEPP calculations.
- Normalized (Kohn-Sham) wave functions from projector augmented wave-based calculations.
- A new scheme for calculating charge carrier lifetimes from first principles.
- A novel design for computing recombination rates using envelope function approaches.

Again, the integration of the various scales was an important common goal in these calculations. Also, a systematic validation scheme to test the modelling set using various experimental techniques on idealized interfaces was an important outcome.

The **fourth objective** of HiperSol was to apply the multi-scale modelling tools to predict improved structures and materials for contacting and passivation in solar cells.

After validation of the modelling tools on simple systems, the methodology was employed on more realistic and practical systems. The HiperSol consortium used this to generate ideas for improving the contacting and passivation interfaces in silicon solar cells. In this way, new structures and materials were screened before conducting expensive and complicated experiments. Thus the following subgoals had to be met:

- Obtain new fundamental insight into the role played by the contacting and passivation interfaces in solar cells (and other semiconductor materials), based on current materials.
- Formulate new structures and materials to improve contacting and passivation schemes.
- Assess the applicability of new materials to industrial production.

The ultimate goal was to combine these modelling efforts with engineering at the nano-scale for improved contacting and surface passivation to enable cheaper and/or more efficient silicon solar cells.

4.1.3 Main S&T results/foregrounds

WP1: Determination of geometric structures

The structure and properties of the contact and passivation interfaces in solar cells have considerable effects on the cell behaviour. Examples include the electronic conductivity across the interface (for example, the effect of Schottky barriers) and the generation of recombination defects. Understanding and predicting these effects requires models of the interfaces at the atomic scale. In principle, it would be desirable to use *ab initio* quantum mechanics to calculate the properties of these interfaces. In practice the number of atoms required to model the interfacial structures adequately is too large (and the number of structures that need to be considered is too high), for this to be possible, even with the recent developments described below. We must therefore use a combined strategy of using simpler, classical models based on force-fields to investigate interfacial structures, reserving the use of *ab initio* methods for particular cases and also using the structures generated by the simpler models as a starting point for the more expensive *ab initio* calculations where possible. It is therefore necessary to develop models using classical force-fields that are of sufficient quality to do this using *ab initio* simulation data as a starting point. Such models must be compared both with further *ab initio* simulations and well-targeted experiments for validation. This is the purpose of the first work-package. The validated models can then be used elsewhere within the project. Models have therefore been developed for both the silicon/metal contacting interface (initially the metal was silver but other metals have also been considered) and silicon/silicon nitride passivation interfaces. This has required the determination of suitable models for the bulk materials and the interfaces from a combination of *ab initio* calculations and experimental data; the generation of suitable interfacial structures at the atomistic scale and the validation of the models using suitable experimental and *ab initio* data where possible. The silicon/silver and silicon/silicon nitride interfaces (the most important for this project) was validated against a combination of *ab initio* and experimental data. The other metals considered (Ni, Zn) were validated against a range of *ab initio* simulations.

For the ***contacting* (*metal/silicon*) *interface***, we have used different models for the bulk materials and developed new models for the interfaces. For the metals we used an embedded atom model, which has been successfully employed for modelling the metals of interest. This takes account of the metallic bonding through a simple many-body function. For Si (and for the interaction between Si and metal) we used the Tersoff force-field that has been widely used for the modelling of Si and can account for the bond directionality characteristic of this covalent material.

The parameters of the model force-fields were first optimised to reproduce the results of *ab initio* simulations using the VASP code. For the Si/Ag interface, this *ab initio* data included the bond length and binding energy of the Si-Ag dimer, the optimized geometry obtained after replacing an Ag atom in the unit cell by a Si atom and the geometries and work of separation calculated for the interfaces Si(111)//Ag(111), Si(110)//Ag(110), Si(100)//Ag(100) and Si(100)//Ag(110). We also compared to structures obtained by *ab initio* methods for the Ag(110)//Si(110) interface and the Ag(100)//Si(110) interface and structural details of calculated AgSi structures taken from the literature. All of our calculated cluster bond lengths are within 5% of the *ab initio* values, although

our potential was based primarily on condensed state data. For other metals, the validation set used was similar.

For the Si/Ag interface, we also compared to experimental data for the structure of the Ag(001) interface with the 2x1 reconstructed Si(001) surface, the Ag(011) interface with the 2x1 reconstructed Si(001) surface and recent high resolution electron microscopy (HREM) results for the spacing of the (111) planes at the Ag(111)//Si(111) interface. The relaxation of surfaces in contact with one another can be characterized by both the interatomic distances at the surface and the inter-layer distances of the surface to bulk layer atoms. These values are available experimentally for Ag surfaces in contact with the reconstructed Si(001)(2x1) surface. In all cases the calculated values are within 3% of the experimental ones. We find the interatomic separations obtained from the force-field to be within 5% of the *ab initio* results and generally good agreement for bond angles. When we compare to recent HREM results for interlayer spacings at the Si/Ag interface in a crystalline Si solar cell, we find that our values are within 0.2% of experiment (i.e. within the spatial resolution of HREM).

We also investigated the geometry of the two interfaces identified by Transmission Electron Microscopy (TEM) using a combination of empirical and *ab initio* methods. For both interfaces it was found that significant re-organization of the atomic positions compared to the ideal crystal positions (> 0.01 nm) occurred only within the first 5 % either side of the interface. For the 111//111 interface there is very little distortion of the surface layer to back layer distances on either side of the interface, with both Si-Si and Ag-Ag bonds being within 0.001 nm of the ideal crystal values. For the 110//110 case, the Si-Si bond between the surface and back layer is slightly stretched relative to the perfect crystal, whilst the Ag-Ag bond is slightly compressed.

In order to provide input and feedback for the metallization process modelling and the calculation of the global conductance at the contact interfaces, the phenomenological reasons for good and bad contact resistance values were studied. Increasing the emitter sheet resistance causes an increased contact resistance. If the electrically inactive excess phosphorus-doping concentration in the emitter is further decreased, fewer Ag-crystallites are grown into the Si surface. As observed by TEM, the excess phosphorus results in considerable strain within the Si lattice that could facilitate Ag crystallite nucleation and growth. Additionally, different Ag-pastes result in different contact formation.

Further details of the use of this modelling can be found under WP3 and WP5.

The generation of the **passivation** layer on top of silicon, the firing process of the contacting layer and graded doping of silicon all lead to diffusion across interfaces and inside the bulk materials. It is thus particularly important to obtain knowledge of the geometric structure of these interfaces and related nearby structures, which will include defects or perturbations of the perfect crystalline bulk structure. Models for the silicon-silicon nitride interface were developed and applied to show the effects of different preparations of the interface (whether abrupt or gradual) on the interfacial defects and hence on the electronic properties.

The different phases of Si_3N_4 were investigated using *ab initio* methods and the P63m found to be the most stable. Models were built for the crystalline-Si//amorphous-Si_3N_4 interface and electronic structure calculations performed for these models. The results are evaluated by detailed comparison

of the force-field models with small models built using a full *ab initio* density functional treatment. In a first step, small amorphous models of the passivation layer were created using *ab initio* and force fields. We found that the previous Tersoff parameterizations result in a too high defect density in amorphous silicon nitride, in particular for stoichiometries different from Si_3N_4. To construct the models necessary to simulate the interface in this project we refined the force-field parameters. The fitting was done by employing the force-matching technique to fit these parameters to *ab initio* molecular dynamics simulations. The agreement with full *ab initio* simulations was satisfactory, in particular for structural properties. The final structures are usually relaxed using *ab initio* methods to guarantee that residual forces do not degrade the calculated electronic properties. The force-field parameterisation which resulted gave structures which, when geometry optimised by *ab initio* methods, gave wider band-gaps than those using published force-fields, indicating fewer defective centres and a better representation of the structure. Unfortunately it proved impossible to reproduce completely a structure that gave the same band gap as a structure generated solely from *ab initio* molecular dynamics. However the new potential parameterization gives more reliable structures than previous parameterizations and was used in the project for work on designing improved passivation layers.

The SiN_x/Si interface was characterized with ellipsometry and SIMS to determine the effect of passivation. This shows that a gradient in composition is important for the passivating quality. The SiN_x signal penetrates inside the first nanometres of the bulk c-Si, which can be interpreted as nitridation of the Si. The difference between passivating and standard SiN_x expresses itself in the Si-N bond density as measured with bulk FTIR, lower for the former, and the refractive index, higher for the former. Both SiN_x layers show a trend through the layer with increasing refractive index. A similar trend can be found with ellipsometry, in which an interface layer can be modelled. For this, different SiN_x layers have been fabricated with similar refractive indices, but with varying Si-N bond densities. Both low and high levels of nitridation will give limited passivation, the optimum can be found in between. This might be related to the balance between the fixed charge (more nitridation will enhance the fixed charge) and induced strain or damage in the first nanometres of the crystalline Si bulk and thus the density of interface states.

Simulations of the nitridation effect show that with increasing nitridation the volume and fraction of important defects in the silicon (K and N centres) increase and are found within a few nanometres of the interface. This correlates well with the experimental results obtained. Further details may be found in other workpackages.

WP2: Atomistic band structures for large systems

Development of computational methods and tools:

The development effort within this work package strongly focused on three key issues that needed to be solved in order to calculate accurate band structures and wave functions for large atomistic models:

1.) A bandgap correction scheme. Since conventional density functional theory calculations massively underestimate the band gap in the materials considered within the project (Si, silicon nitride, glass). The band gap error greatly complicates the prediction of the properties of defects and interfaces and needs to be dealt with before we can seriously consider calculations for large models.

We have adopted a band-gap correction scheme, the modified Becke-Johnson local density approximation (MBJLDA), that has now been tested for III-V semiconductors as well as Si, silicon nitride and silicon oxide. The scheme yields accurate band gaps for all considered materials, although, as expected, it involves a grain of empiricism, requiring adjustment of the parameters against high level quasiparticle calculations such as GW. To illustrate the aforementioned, Fig. 2 shows a comparison between the MBJLDA and GW results for the bandstructure and density of states of β-Si_3N_4.

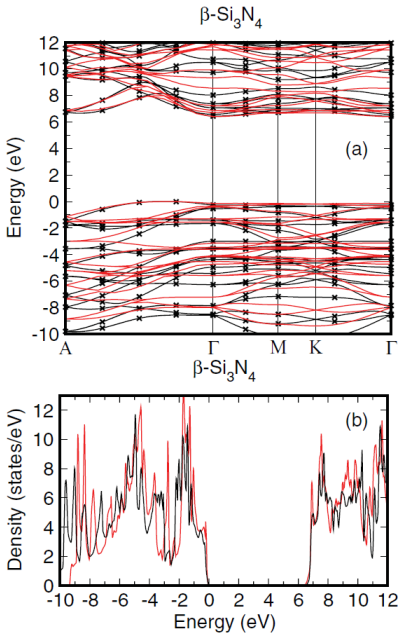

Figure 2: *(a) Band structure and (b) electronic density of states of β-Si_3N_4. The sc-QPGW results are shown as black lines, while the MBJLDA results are represented by red lines.*

2.) Development of fast iterative matrix diagonalization methods for the calculation of electron and hole band structures in large systems containing several hundred thousand atoms. This objective was achieved by constraining the calculations to selected orbitals around the valence band maximum and conduction band minimum. These states are relevant for the electronic and transport properties. We implemented a robust and very efficient scheme, the harmonic Davidson inner eigenvalue solver, and the method has been applied to and evaluated for systems containing up to 100 000 atoms. Fig. 3 shows the density of states in and around the bandgap in a 1000 and a 100.000 atom cell of Si_3N_4, obtained using the harmonic Davidson inner eigenvalue solver (red and green lines). For the 1000 atom system, the result from a standard DFT calculation were all orbitals are computed, is shown as well (black line).

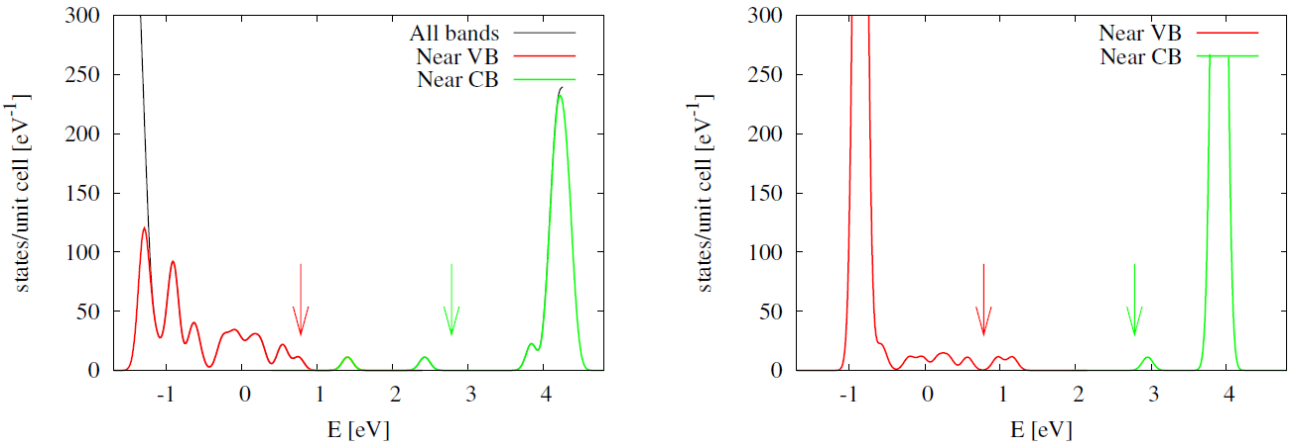

Figure 3: *Density of states (DOS) for the 1k- and 100k-Si_3N_4 system (left and right panels, respectively). For the 1k system, the black line is the result from a standard DFT calculation. The colored lines are obtained using the harmonic Davidson inner eigenvalue solver, and were determined in two separate runs, with reference energies ε_{ref} at the positions indicated by the arrows. The zero of the energy axis is set to the Fermi energy.*

3.) Effective semi-empirical potentials for non-selfconsistent calculations. When the calculations are constrained to few states close to the Fermi level, the potential created by the other valence electrons can no longer be calculated parameter free. This implies that we need to account for the effect of the other electrons be means of an effective screened semi-empirical potential. We achieved this goal by adopting a new charge-fit procedure, in which the electronic density distribution of the valence electrons is fitted to amorphous model structures. As is illustrated in Fig. 4, this allows us to reproduce the DFT or GW band structure of bulk materials with very good precision without the need for selfconsistency.

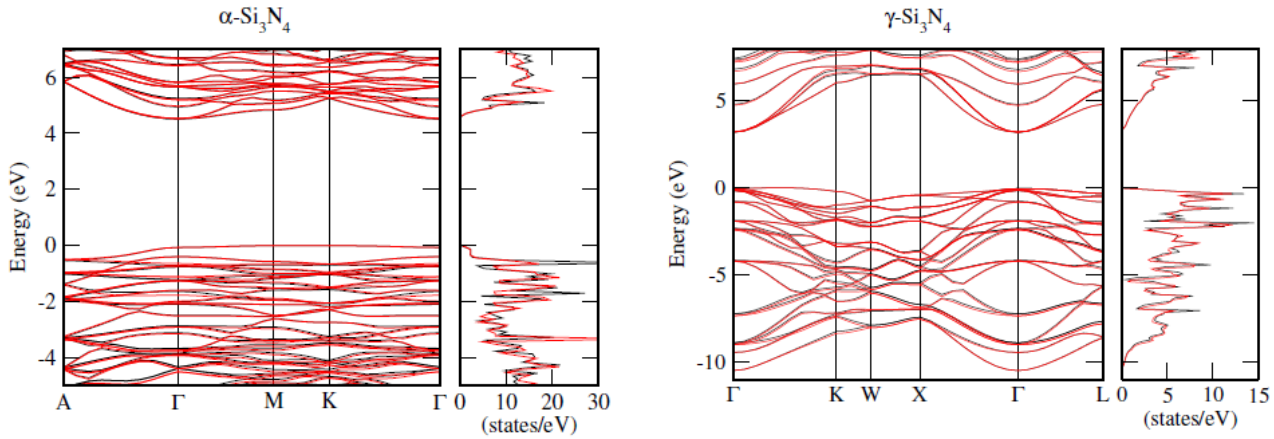

Figure 4: *The bandstructure and DOS of α-Si_3N_4 and γ-Si_3N_4: calculated selfconsistently (black lines) and non-selfconsistently using Gaussian charge-transfer charges from amorphous- Si_3N_4 (red lines).*

In addition to the three points mentioned above, we have invested considerable effort in:
4.) The implementation of an efficient scheme to calculate Auger recombination rates from DFT orbitals. The ab initio calculation of Auger recombination rates requires a very dense sampling of the first Brillouin zone in reciprocal space, to such an extent even that the selfconsistent DFT calculations that serve as input become prohibitively expensive. Therefore, in addition to the evaluation of the Auger recombination rates, we have implemented an interpolation scheme that

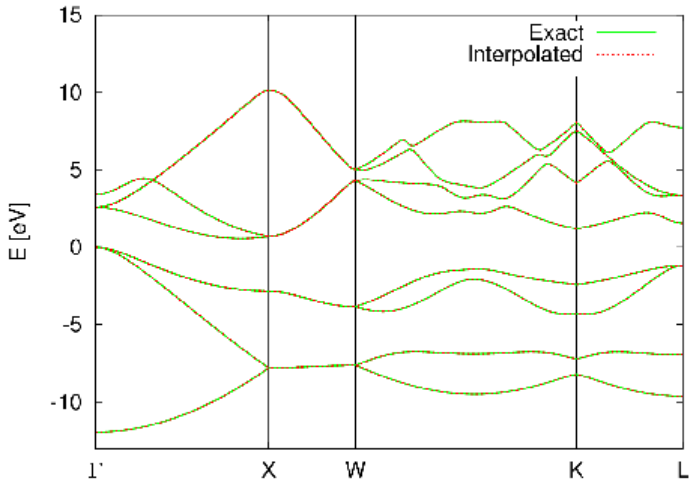

Figure 5: *Band structure for silicon using an exact calculation (charge density taken from a 24×24×24 k-mesh) and an interpolation from a 6×6×6 k-mesh. The energy differences are in the meV range.*

Table 1: *Auger recombination rates in n-Si from GW calculations on a 12×12×12 grid of k-points.*

Electron density n_0 [cm^{-3}]	Auger lifetime τ_{eeh} [s]
10^{16}	2.39×10^{-1}
10^{17}	2.39×10^{-3}
10^{18}	2.39×10^{-5}
10^{19}	2.39×10^{-7}
10^{20}	2.39×10^{-9}

allows for the construction of the one-electron orbitals at a very dense mesh in reciprocal space from an underlying calculation on a coarse grid of points in reciprocal space. Both features (calculation of Auger recombination rates as well as the interpolation algorithm) will be useful in many application far beyond the scope of the HiperSol project.
To illustrate our interpolation scheme, Fig. 5 shows a comparison of the bandstructure of Si from a DFT calculation using a 24×24×24 mesh of **k**-points and the corresponding interpolation from an underlying 6×6×6 **k**-mesh. Results for the Auger recombination rates in n-type Si are listed in Tab. 1.

Applications

In terms of the application of our computational methods and tools, the main achievement within this work package was the identification of the dominant defects in bulk amorphous-$Si_3N_{4-x}H_y$ and crystalline-Si/amorphous-$Si_3N_{4-x}H_y$ interfaces and the characterisation of the contributions of these defects to the density of states within the bandgap. The role of hydrogen as passivator of the dangling bonds of under-coordinated atoms has been elucidated. The mechanism that leads to so-called "fixed-charges" at the silicon nitride side of the c-Si/ a-$Si_3N_{4-x}H_y$ interfaces is now understood at the atomistic level.

1.) Defects in bulk amorphous-$Si_3N_{4-x}H_y$:

First of all, we constructed a statistically sound ensemble of amorphous-$Si_3N_{4-x}H_y$ structures (actually a-Si_3N_4, a-$Si_3N_{3.5}H_{0.8}$, and a-$Si_3N_3H_{0.8}$) using ab initio molecular dynamics (MD) techniques (roughly 1000 independent samples for each stoichiometry). These samples were analysed with respect to the number and the nature of the defects they contain, and the influence of these defects on the electronic structure.

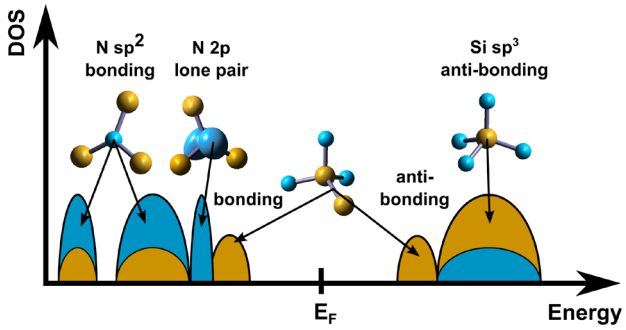

(A)

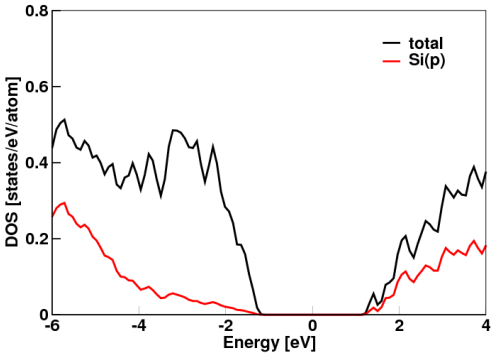

(B)

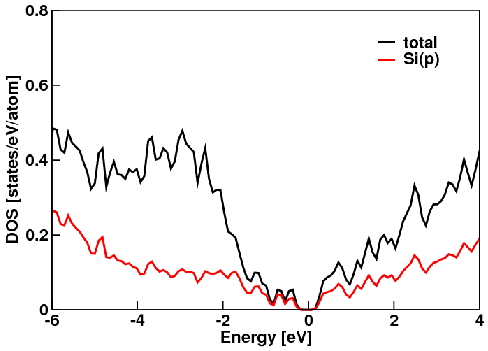

(C)

Figure 6: ***A)*** *Schematic representation of the density of states in a-Si_3N_4. The bonding complexes are indicated (blue: N, yellow Si).*
B) and C) *The statistically averaged density of states in a-Si_3N_4 and a-Si_3N_3, respectively. Note the increase in the density of states within the gap with decreasing N content. These states stem from Si-Si pairs/Si clusters: sp^3 bonding states at the top of the valence band and anti-bonding contributions near the bottom of the conduction band.*

Si in crystalline and amorphous Si exhibits tetragonal (four-fold) coordination (Si-Si_4) and sp^3 hybridization. Its electronic structure shows an energy gap (about 1.2 eV) between the valence band (Si sp^3 bonding) and conduction band (Si sp^3 anti-bonding). Si_3N_4 phases (α-, β- and the amorphous phases) are wide gap insulators (energy gaps > 5.0 eV). In Si_3N_{4-x}, Si atoms are still in a tetragonal coordination, and N atoms triangularly (three-fold) coordinated. The valence band is dominated by N sp^2 hybrid (bonding) orbitals at lower energy and N lone-pairs (non-bonding) at the upper part of the valence band. The conduction band is composed of Si sp^3 anti-bonding states (see the schematic representation in Fig. 6A).

In amorphous (a-)Si_3N_{4-x}, both Si and N atoms would prefer, topologically speaking, to keep their tetragonal- and triangular-coordinations in a distorted Si-N network, respectively. Naturally the distortions causes states to tail into the band gap increasing the number of states in the gap. The major structural defects in a-Si_3N_4 are under-coordinated Si (Si-N_3) and N (N-Si_2), which are known as K-defects and N-defects, respectively. The K-defects contribute dominantly to the defect states in the middle of the energy gap. With decreasing N concentration in a-Si_3N_{4-x}, Si-Si pairs or Si-clusters appear due to the deficiency of N atoms. These Si-Si pairs/Si clusters contain sp^3 bonding characters with states at the top of the valence band and anti-bonding contributions (bottom of the conduction band), as shown in Fig. 6. Consequently, the energy gap of a-Si_3N_{4-x} decreases with increasing x (compare Fig. 6 B and C). Our analysis shows that K-defects and Si-clusters are the most relevant defect-states withinin the energy gap. In addition we find that H atoms serve to passivate the under-coordinated Si atoms. The latter is illustrated in Fig. 7, undercoordinated Si and N are effectively passivated, whereas the defect density of states stemming from distorted ideally coordinated (SiN_4 and NSi_3) structural units is hardly affected. In addition, Fig. 7 shows that the defect density is strongly affected by the cooling rate of the MD procedure used to construct the a- Si_3N_{4-x} structures (fast: "quenched", or slow:"cooled").

2.) Defects near the crystalline-Si/amorphous-$Si_3N_{3.5}H_{0.8}$ interface

Again, by means of ab initio MD we constructed over 1000 c-Si/a-$Si_3H_{3.5}H_{0.8}$ interface structures. The ensemble of interface structures was carefully analyzed with respect to (i) the number and nature of the defects in the silicon nitride part of the system, and in the c-Si near the interface, (ii) the electronic properties of these defects, foremost their contribution to the density of states within the gap, (iii) the spatial distribution of H, and (iv) the influence of the presence of H on the density of states in the gap.

Fig. 7 shows a typical example of a c-Si/a-$Si_3H_{3.5}H_{0.8}$ interface, and labels a few H passivated K defects (labeled K*) and an unpassivated K defect, i.e., undercoordinated Si sites.

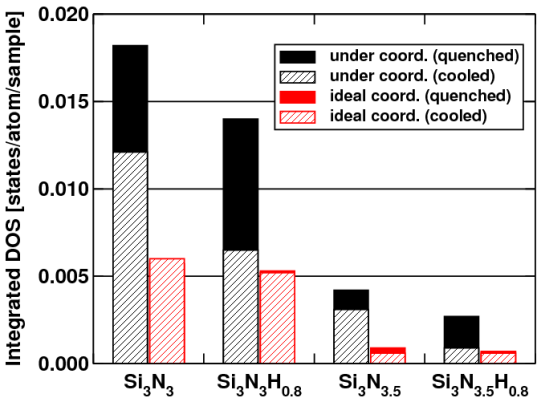

Figure 7: *The influence of H on the defect density of states in a-Si_3N_{4-x}. Undercoordinated Si and N are effectively passivated, whereas the defect density of states stemming from distorted ideally coordinated (SiN_4 and NSi_3) structural units is hardly affected.*

The defects that we find in these interface structures are of the same nature as the defects we encountered in the bulk a-$Si_3N_{4-x}H_y$ structures: undercoordinated Si (threefold) and N (twofold), and ideally coordinated but strongly distorted SiN_4 and NSi_3 units. The undercoordinated defects are in part passivated by H.

Fig. 8 shows a close-up of the ensemble averaged density of states around the Fermi-level. As is evident from Fig. 8, the defect induced states within the gap are mainly due to undercoordination defects (black lines), and only to a much smaller extent due to distorted ideally coordinated bonding units (red lines). The presence of H has hardly any influence on the density of states within the gap (compare the drawn lines with the dashed).

Two thickly drawn red lines indicate the top of the valence band (left thick red line) and the bottom of the conduction band (right thick red line) on the c-Si side of the interface. The defect states between these lines (almost exclusively located at the silicon nitride side of the interface) play an important role in the defect assisted carrier recombination of electrons and holes created on the c-Si side of the interface.

In addition to the dashed vertical black line in Fig. 9, that indicates the Fermi-level of the amorphous silicon nitride subsystem, we have indicated an estimate for the position of the Fermi-level at the crystalline silicon side of the interface as well (red vertical line). In practice, of course, the Fermi-levels on both sides of the

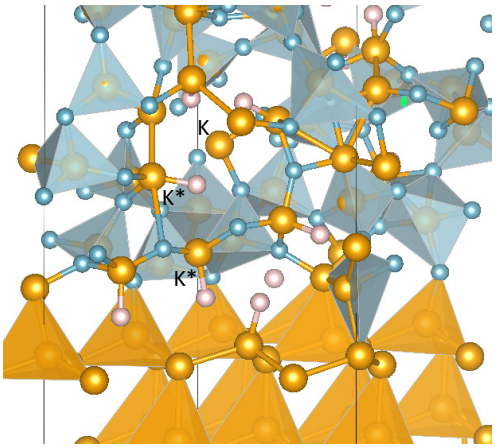

Figure 8: *Typical example of a c-Si/$Si_3H_{3.5}H_{0.8}$ interface (blue: N, yellow: Si, white: H). With K* we have labeled two defects made up of undercoordinated Si atoms passivated by H. The label K labels a classical (non-passivated) undercoordinated Si.*

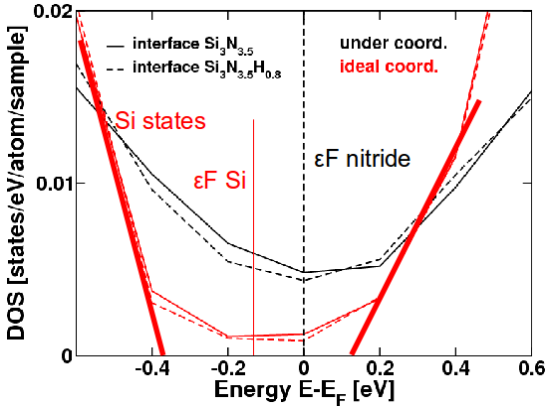

Figure 9: *Close-up of the ensemble averaged DOS around the Fermi-level in c-Si/a-$Si_3H_{3.5}H_{0.8}$. Defect induced states within the gap are mainly due to undercoordination defects (black lines), and to a much smaller extent due to distorted ideally coordinated bonding units (red lines). The presence of H has hardly any influence on the DOS within the gap (compare the drawn lines with the dashed). The thickly drawn red lines indicate the top of the valence band (left thick red line) and the bottom of the conduction band (right thick red line) on the c-Si side of the interface.*

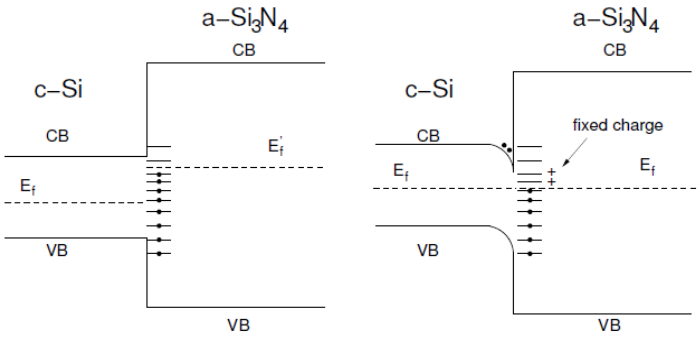

Figure 10: *Schematic representation of the band realignment between the c-Si and a-Si_3N_4 sides of the interface. Before band realignment (left): the Fermi level at the a-Si_3N_4 side of the interface lies higher than on the c-Si side. In practice, the Fermi-levels on both sides of the interface will be equilibrated: charge flows from the a-Si_3N_4 side of the interface into the c-Si part, depleting a number of defects states in a-Si_3N_4, and introducing a number of electrons into the c-Si conduction bands. After band realignment (right): these depleted defect states at the a-Si_3N_4 side of the interface represent positive charges (often called the "fixed charge").*

interface will be equilibrated: charge will flow from the silicon nitride side of the interface into the silicon part, depleting a number of defect states near the interface and injecting electrons into the c-Si conduction bands.

These depleted defect states at the silicon nitride side of the interface represent positive charges (often called the "fixed charge"). This process is illustrated in Fig. 10.

WP3. Modelling of contacting interface

Atomistic calculations:

DFT based molecular dynamics (MD) was used to simulate the various phases and interfaces relevant for the FEM study. Since most of the phases were in the liquid state, it was possible to use elevated temperatures for many of the systems. Nevertheless, we have obtained results for all relevant diffusion parameters at 1000 K, which is a relevant temperature for the firing process.

Diffusivities were calculated by first-principles molecular dynamics. Results with and without silver are shown in Figure 11. The diffusivities of each element were fitted to an Arrhenius behaviour;

$$D(T) = D_0 \exp\left[-E_a/RT\right], \quad (1)$$

where D_0 is the prefactor, E_b is the energy barrier, R is the gas constant, and T is the temperature.

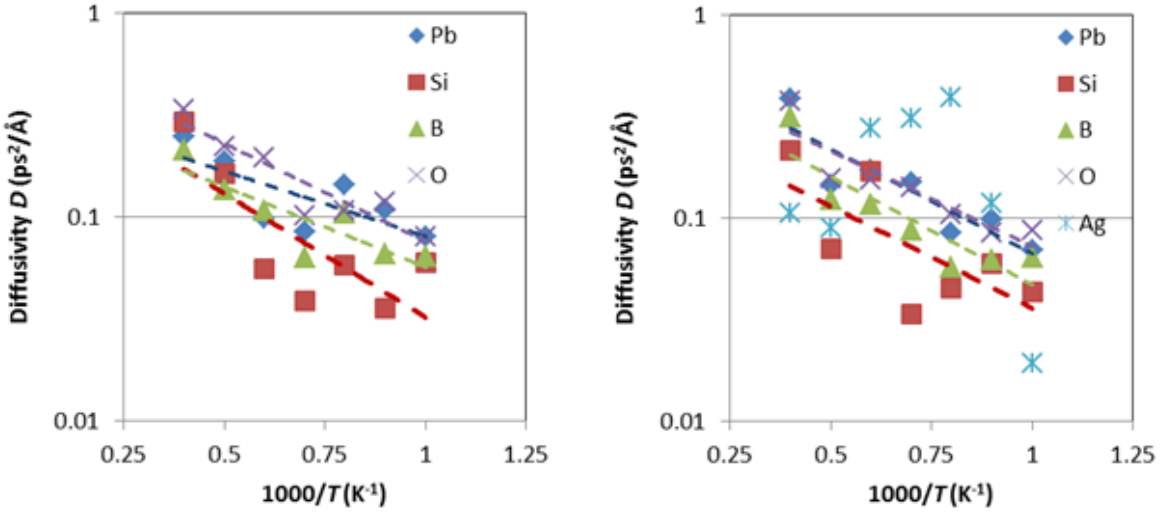

Figure 11. *Calculated diffusivities as a function of temperature in an Arrhenius plot. Glass 3 without (a) and with (b) dissolved silver is shown (the scatter for Ag is due to short simulation time.). The dashed lines are best fits to an Arrhenius behaviour.*

The force fields obtained from WP1 (D1.2) were used to simulate the Si/Ag contacting interface. The (111//111) and (110//110) interfaces, which were identified in samples as part of D1.1 were simulated. The potentials were used to search through a large number of possible starting configurations and identify the most suitable candidates for simulation using density functional theory (DFT). The DFT simulations reveal metal-induced gap states (MIGS) in the density of states plots at the Si/Ag interface, (Figure 12).

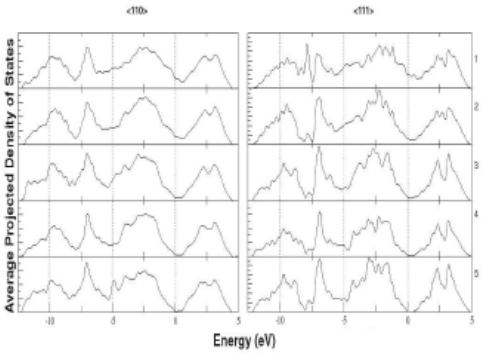

Figure 12. *Averaged projected density of states of the Si atoms in each layer moving away from the Si/Ag interface from the top down. The supercell Fermi level is set to zero.*

The Schottky barriers were calculated for silver contacting to pure Si and to Si doped with phosphorus, highlighting the role of phosphorus for reducing the SBH. The SBHs were also calculated for Si/Ni (silicide) interfaces and Si/Zn interfaces. It was found that the Schottky barriers vary considerably with the type of Ni silicides. Zn was found to have a higher SBH, even in the presence of doping. These results are presented in table 2.

Table 2: *The calculated Schottky barriers at different interfaces and under different doping condidtions*.

Metal	Si Surface	Metal Surface	Doping/cm3	n-SBH/eV	p-SBH/eV
Intrinsic Si					
Ag	100	100	-	0.41	0.71
Ag	110	110	-	0.52	0.58
Ag	111	111	-	0.74	0.36
Ag	112	112	-	0.65	0.47
Phosphorus Doped					
Ag	100	100	1.20E+20	0.37	0.73
Ag	110	110	1.20E+20	0.36	0.64
Ag	111	111	1.20E+20	0.52	0.58
Ag	112	112	1.20E+20	0.51	0.61
Boron Doped					
Ag	100	100	1.20E+20	0.81	0.31
Ag	110	110	1.20E+20	0.78	0.34
Ag	111	111	1.20E+20	0.71	0.41
Ag	112	112	1.20E+20	0.81	0.31
Intrinsic Si					
Ni	100	100	-	0.69	0.43
Ni	110	110	-	0.52	0.60
Ni	111	111	-	0.70	0.42
$NiSi_2$	100	100	-	0.54	0.58
$NiSi_2$	110	110	-	0.50	0.62
NiSi			-	0.54	0.58

Ni_2Si			-	0.66	0.46
Phosphorus Doped					
Ni	100	100	1.20E+20	0.39	0.73
Ni	110	110	1.20E+20	0.46	0.66
Ni	111	111	1.20E+20	0.53	0.59
$NiSi_2$	100	100	1.20E+20	0.54	0.58
$NiSi_2$	110	110	1.20E+20	0.45	0.67
NiSi			1.20E+20	0.58	0.54
Ni_2Si			1.20E+20	0.59	0.53
Intrinsic Si					
Zn	111	001	-	0.86	0.26
Phosphorus Doped					
Zn	111	001	1.20E+20	0.67	0.45

We also investigated the role of P for promoting the formation of Ag crystallites at the Si surfaces. Using classical nucleation theory (CNT) we were able to show that the P stabilises the Si/Ag interface. We show that the rate of nucleation depends on the nature of the glass frit used. The results for nucleation rates at the (110)/(110) and (111)/(111) interfaces are presented in figure 13.

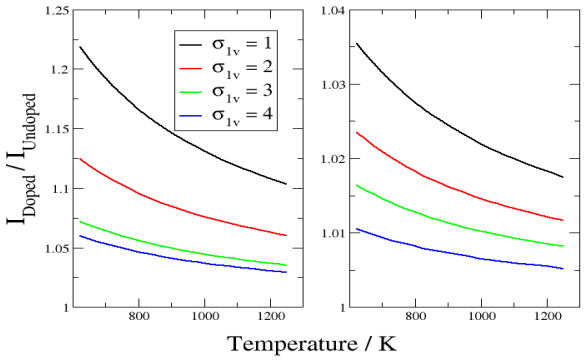

Figure 13. *The ratio of nucleation rates for a range of Ag-Glass interfacial energies (σ_{1v}) at the doped and undoped interfaces for the (111) Si-Ag interface (left) and the (110) Si-Ag interface (right).*

Theoretical results for the Schottky barriers for the following interfaces were implemented together with n-doped Si: Ag(111), Ag(110), Ag(100), Ag(112), Ni(100), Ni(110), Ni(111), $NiSi_2$(100), $NiSi_2$(110), NiSi, Ni_2Si, Zn(111). Furthermore, the Ag(111)-pSi interface was also implemented.

In addition we have investigated the effects of phosphorous doping on the barriers at the Si/Ag interface. The first step in this investigation has been to decide the preferred location of P doping at the interface. The results of this investigation (figure 14) reveal that in both cases the P is more favourable at the upper layers, close to the interface. At the 110 interface there is little difference between layer 1 and layer 2, but in both cases the substitution becomes significantly less favourable as we move towards the bulk.

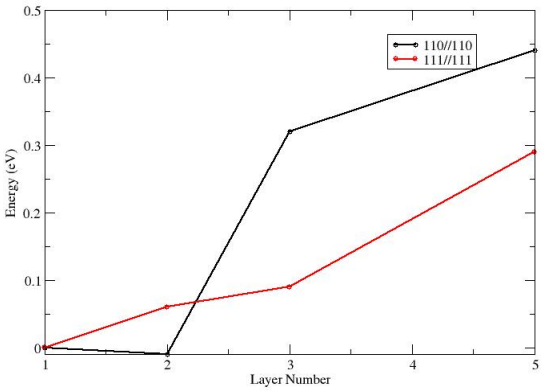

Figure 14: *Energies of P doping of Si at the Si/Ag interface. In both cases energies are offset to the energy of layer 1. The layers are listed in ascending order moving away from the interface.*

Continuum calculations:

The work has consisted of i) establishing necessary thermodynamic model input, phase-diagrams and Gibbs free energies; ii) solving the diffusion equation in the liquid phase for equilibrium and non-equilibrium surface conditions and solving the mass balance at the particle surface; and iii) establishing and solving the phase-field model in the commercial software Comsol Multiphysics. Qualitative agreement between the models ii) and iii) has been obtained. Quantitative correspondence will be discussed below.

The physical process for the metallization process that has been investigated is the thermodynamic non-equilibrium situation that allows for a solid substance to be dissolved into a liquid at temperatures below the melting temperature of the solid.

The driving force of dissolution is the temperature dependent chemical potential gradient. The same mechanism allows for precipitation of solids from the liquid phase.

The mathematical model consists of the coupled Allen-Cahn and Diffusion equations, for the order parameter and solute mole-fraction, respectively;

$$\frac{\partial \varphi}{\partial \tau} = \frac{M_\varphi \varepsilon^2}{D} \nabla^2 \varphi - P \frac{\partial G_{mix}}{\partial \varphi} \quad , \tag{1}$$

and

$$30\left(z_{S,0} - z_L\right)\varphi^2\psi^2 \frac{\partial \varphi}{\partial \tau} + p(\psi)\frac{\partial z_L}{\partial \tau} = \nabla\left[\, p(\psi)\left(p(\varphi)z_{S,0} + p(\psi)z_L\right) \cdot \nabla \mu_L'(z_L)\right] \quad , \tag{2}$$

Key model input parameters are the diffusivity of solute in the solvent, the surface energy and the interface mobility. In addition, a thermodynamic model and the time-dependent temperature profile are needed. This study was limited to infinite surface reaction rate, giving close-to-equilibrium solute concentration at the particle surface, and the interface mobility can be expressed as

$$M_{\varphi,eq} = \frac{D}{2\varepsilon^2}\frac{z_{L,eq}}{1-z_{L,eq}} \quad . \tag{3}$$

The model was utilized to study aspects of dissolution of spherical particles. E.g. in Figure 15 it can be seen how the time-dependent particle radius behaves depending on the content of the solvent (lead or bismuth).

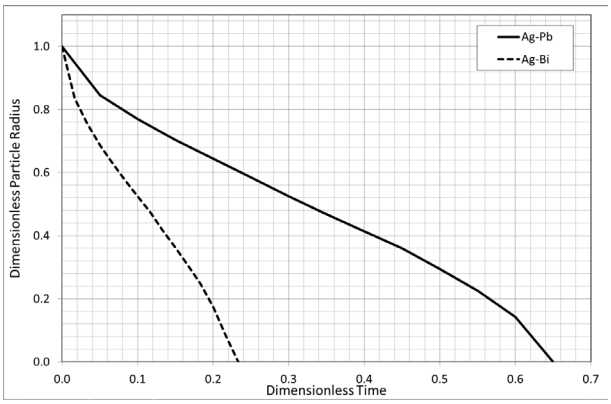

Figure 15. *Comparison of the time-dependent particle radius for a silver particle submerged in liquid lead (solid) and bismuth (dashed), at T=600°C, and M_ϕ=M_{eq}.*

To study the metallisation process, a simplified approach is taken. It is assumed that silver particles are initially residing on top of the SiN layer, as indicated in Figure 16. It is assumed that the liquefied glass etches away the SiN layer, such that the silver particles are separated from the silicon wafer by a liquid film consisting of liquid glass. Further simplification considers the silver particles as an infinite continuous solid silver body, as shown in Figure 17. Eqs. (1) and (2) can now be solved in 1-dimensional Cartesian coordinates to simulate the metallisation process.

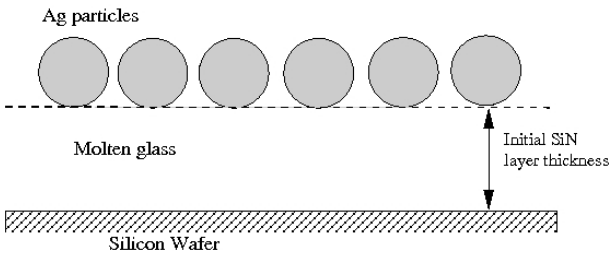

Figure 16. *Simplified model of solid silver particles initially arranged on top of the SiN passivation layer. After the etching of the SiN layer, by the molten glass phase, silver solute needs to be transported by diffusion to the Si wafer surface, to establish electrically conducting paths.*

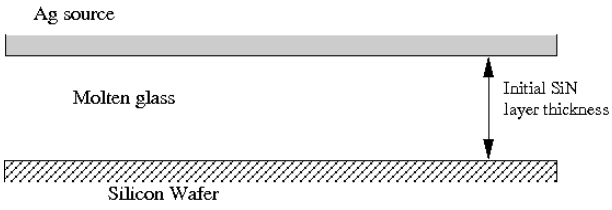

Figure 17. *Homogenization of the simplified picture in Figure 16; the array of spherical silver particles is viewed as a continuous flat silver body, reducing the problem to a 1-dimensional problem in Cartesian coordinates.*

To facilitate the precipitate growth at the silicon surface, when the firing temperature is dropping, an artificial nucleation site is introduced by specifying the existence of a solid silver phase ($\varphi = 1$ boundary condition) at the silicon surface.

To enable modelling of complex liquid mixtures, a thermodynamic procedure was developed to reducing the multicomponent glass phase to a single pseudo component. Output from the procedure was the concentration and phase dependent Gibbs free energy and saturation point for a mixture of solute and the glass phase.

Experimental validation and input:

Phenomenological studies were conducted to generate input parameters for the FEM model of the contacting interface to predict the global contact resistance. This part was done in close connection to WP5. To evaluate the relative importance of the possible current transport paths from the Si emitter into the Ag-finger bulk, microscopic contact characterization by SEM was combined with liquid conductive silver application to different stages of etched-back contacts. The corresponding global contact resistance measurements in Table 3 on a typical monocrystalline industrial Si solar cell show that the major current flow into the Ag-finger is through the Ag-crystallites grown into the Si emitter in direct contact with conductive silver, see cases c) and e) in Table 3. Only a minor current flows through the glass into the conductive silver, case b). SEM microscopy after selective silver removal only, see Fig. 18, reveals imprints of etched-away Ag-crystallites at glass-free pyramid tips, which thus have been in direct contact with the Ag-finger bulk beforehand.

Table 3: *Contact resistance measurements after different contact etch-backs and liquid conductive silver application.*

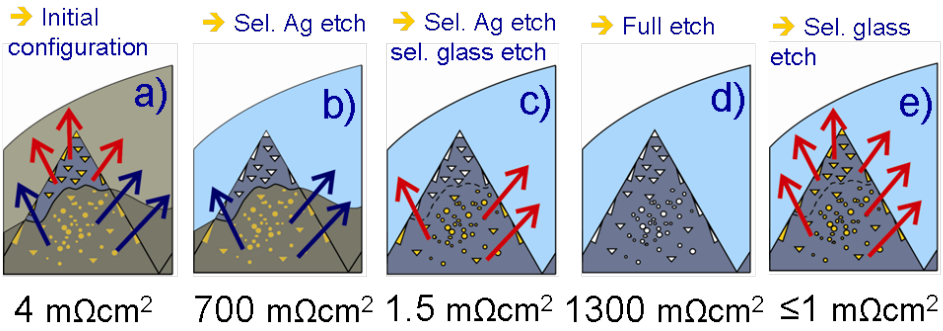

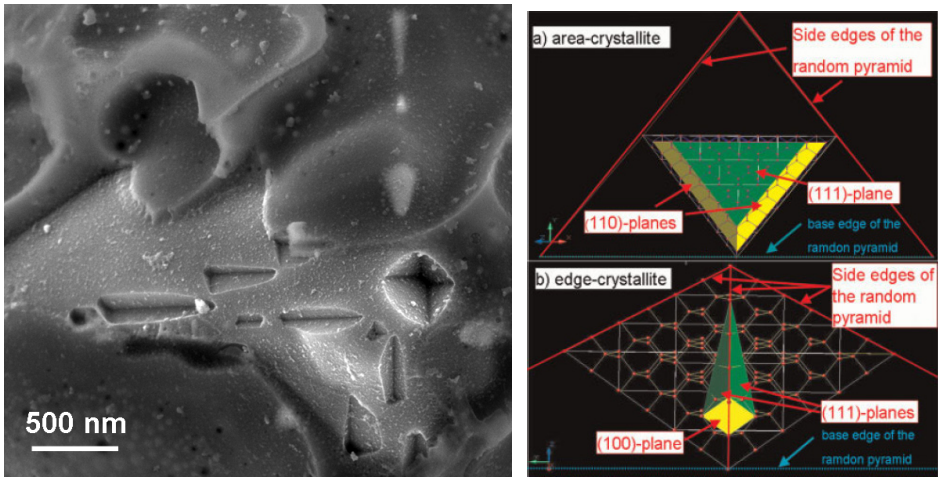

Figure 18: a): *SEM picture showing Ag-crystallite imprints of direct contacts at a glass-free pyramid tip. b): Geometry of Ag-crystallites grown into pyramidal textured monocrystalline Si [Pysch, ProgPhot09]*.

Comparative experiments on flat Si reveal a very sparse direct contact density as the source for the high contact resistivities measured. We conclude that the observed direct contacts are essential for the current transport in silver thick film metalized Si solar cells and the first parameter to calculate for modelling the current transport is therefore the Si-Ag interface resistivity of the observed geometries, see Fig. 18. Besides the already calculated crystal orientation dependence of the Schottky barrier, its value will also be depth-dependent because of the varying P-doping

concentration in the emitter, see Fig. 19a, where the Ag-crystallites penetrate up to ~80 nm in average.

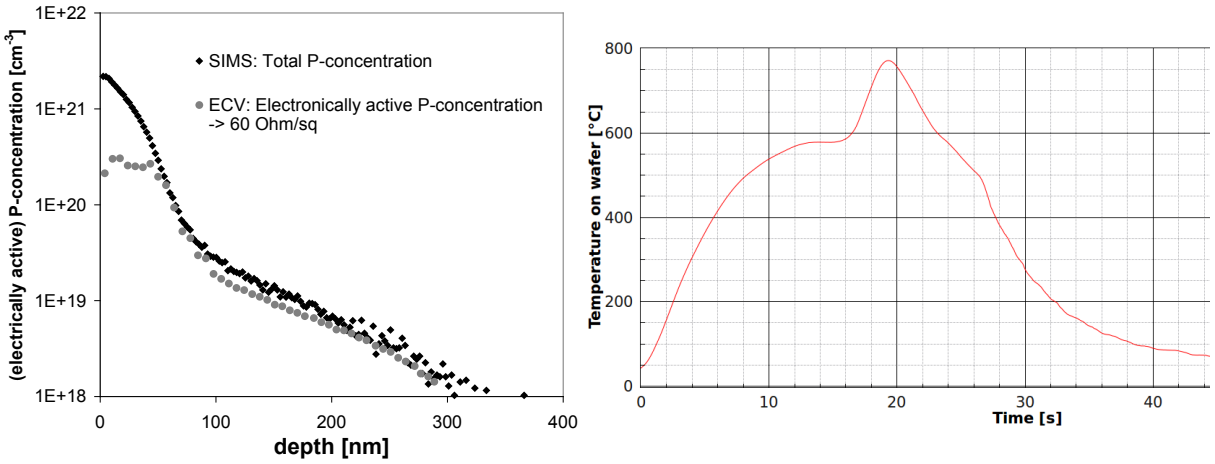

Figure 19: *a) Typical industrial emitter profile. b) Typical metallisation firing profile.*

Regarding the dynamic contact formation, the most relevant experiments shedding lights on the metallization process have been already done, mostly by Gunnar Schubert:

Silver – silicon: Pure silver is able to grow Ag-crystallites into Si with the typically observed geometrical shapes, see Fig. 11, but only at much higher temperatures and longer times than the ones used in a standard firing process, see Fig. 12b.

Glass – silicon: Lead borosilicate glass is observed to etch into Si and results in metallic lead precipitates in the glass: $2PbO + Si \rightarrow 2Pb + SiO_2$. Interestingly, instead of the well-defined Si crystal orientation dependent geometrical shapes in which the Ag crystallizes into the Si surface, see Fig. 19, lead borosilicate glass alone etches Si isotropically leaving round etch pits. Because metallic lead does not wet silicon, the lead precipitates move away from the Si surface in form of spherical crystallites.

Silver – glass → Silver containing glass – silicon: Lead silicate glass is able to dissolve silver. Thus silver saturated lead borosilicate glass on silicon is fired. Instead of the round etch pits from silver-free glass only, the usual pyramidal etching behaviour is observed. Thus, a possible silver growth mechanism could be an anisotropic redox reaction of the silver ions in the glass with silicon, similar to the PbO-Si reaction. As simultaneously Pb precipitates are observed in the bulk of the glass, both redox reactions could occur during the firing process. However, the dissolution of Ag in glass is slow and thus the silver growing in Si must mainly be transported through the glass, as occurring by liquid lead melting silver and forming the experimentally detected liquid silver-lead phase.

Silver – glass – silicon: Again, only minor Ag amounts added to glass are necessary to anisotropically etch silicon. The lead content of the resulting crystallites grown into Si decreases with increasing Ag content in the paste, and crystalline lead is not present in the glass any more. These experimental observations (Schubert's PhD) including measurements of reaction temperatures during firing (also in Hörteis' PhD) are an excellent database to validate the metallisation process model, not only as a whole but also in its subsystems.

As we observed the glass-freeness of the standard monocrystalline Si pyramid tips to be crucial for direct contact formation and thus current conduction, the Ag-paste's wetting properties on different Si surface topographies, see Fig. 20, are experimentally investigated.

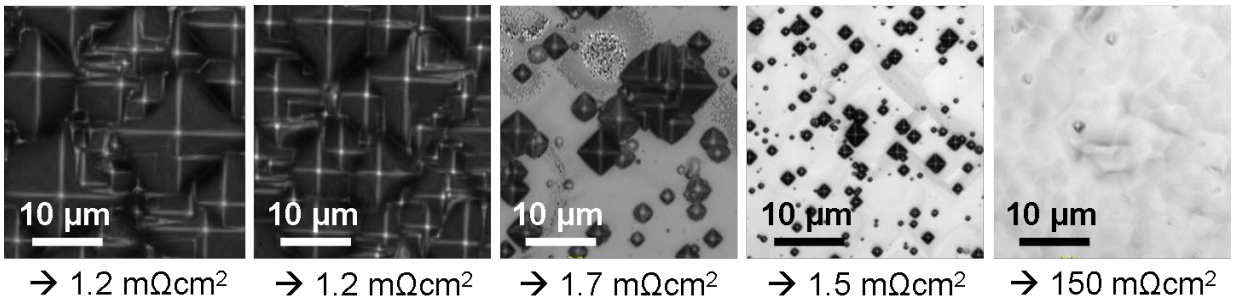

Figure 20: *Dependence of contact resistance on surface topography due to wetting.*

Surprisingly, the formation of very small pyramids on only a part of an otherwise polished surface is sufficient to dramatically lower the contact resistance by two orders of magnitude, see Fig. 20. SEM investigations confirm the formation of directly contacted Ag-crystallites also at these pyramid tips of inferior height. Thus, surface energies play a major role for the successful contact formation during the metallisation process.

The Si/Ag paste interface was also studied by transmission electron microscopy. For screen printed and fired Ag paste on polished (001)Si or textured {111}Si the situation is mainly the same. There are very few direct contacts between the Si crystal and the sintered Ag bulk. However, these direct contacts are of major importance for the contact resistance, but are described in WP5 However, most of Si surface is separated from the Ag bulk by a glass layer with varying thickness. The thickness of the glass layer can be anything from a few nm to hundreds of nm. For textured {111}Si the glass layer is typically thickest between the pyramids and the thickness decreases by approaching the peak of the pyramids. Furthermore, pores of N_2 gas after etching of the Si_3N_4 layer are frequent in the glass layer.

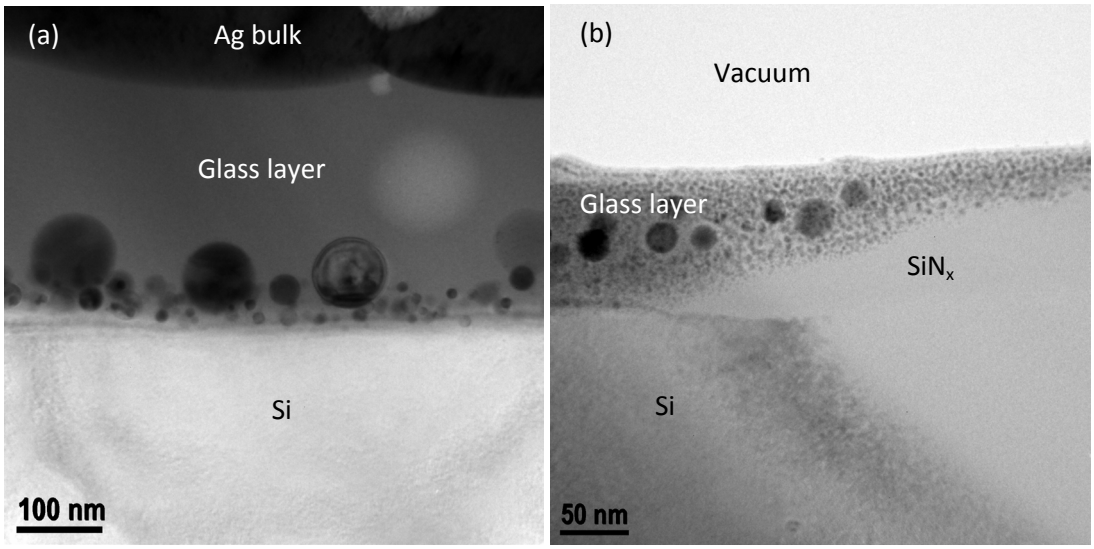

Figure 21. *(a) A thick glass layer is separating the Ag bulk and the Si wafer. Crystalline Ag particles gather close to the Si-glass interface. (b) At thin areas the detailed structure of the glass layer can be seen. Small Pb crystals and "large" Ag crystals are dispersed in the glass matrix.*

The glass layer is not a homogeneous glass, but an SiO_{2-x} matrix with crystals of Ag and Pb dispersed in this matrix. For thick glass layers the Ag crystals gather close to the Si crystal (Fig. 21a) and the size of the Ag crystals can be anything from a few nm to 200 nm. The Pb crystals are much smaller than the Ag crystals with sizes typically in the range 2 – 10 nm (Fig. 21a and 22). Both the Ag and Pb crystals have a face centred cubic crystal structure. The exact stoichiometry of the SiO_{2-x} matrix (the value of x) cannot be determined by high accuracy by TEM, but based on energy

dispersive spectroscopy (EDS) x seems to be close to zero. At some locations, Zn can also be found in the glass layer. However, it is not clear if Zn is in an amorphous or crystalline state or if it is in the form of pure Zn, ZnO or something else.

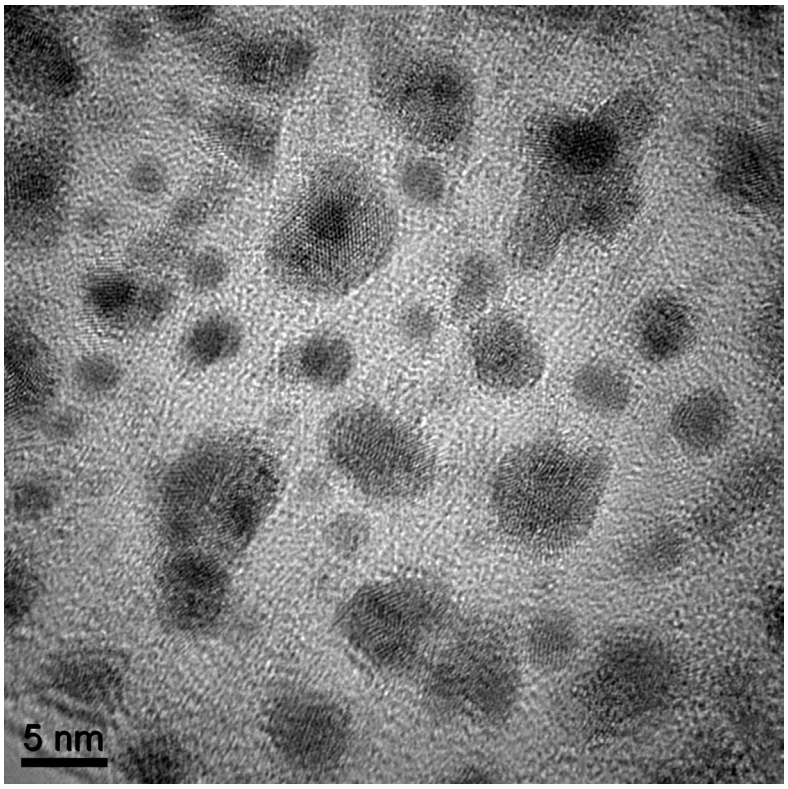

Figure 22. *High resolution TEM image that shows the small Pb crystals that are dispersed in the glass matrix.*

WP4: Modelling of the passivation interface

Several models were generated for studies of Si/SiN_x interfaces regarding the number of potential defects which can act as charge carrier recombination centres. The bonding at the interface between amorphous SiN_x and crystalline Si with various values of nitrogen content x for topological information were investigated using these models. We demonstrated how the concentration of geometric defects at the interface depends on the stoichiometry of the SiN_x layer. It was further shown that a nitrogen concentration gradient across the interface can significantly lower the number of under-coordinated Si defects in the interface region. These results have implications for the design of SiN_x layers for use as passivation/anti-reflective layers in solar cell devices. The information will be further used for solar-cell optimization.

Solid state diffusion across the passivation interface and inside the bulk materials of solar cells can take place both during steady-state operation and accelerated during the firing process of the contacting layer. This will cause defects and modifications to the interfaces. We have combined Nudged Elastic Band (NEB) and First-principles molecular dynamics (FPMD) methods to study the detailed diffusion mechanisms and defect formation processes. We further investigated the impact of various defects on the performance of the solar cell for which we needed detailed knowledge of the defect-free bulk and interface structures. In this respect we wanted to obtain knowledge of the electronic properties of Si_3N_4. The studies are very demanding, but also valuable, since they complete the view of the conduction process, e.g., defect levels, exciton effects, screening, etc. These

results will be important for the lifetime calculations and are benchmark studies in the field of solid-state calculations.

As we concentrated on studying the recombination losses of photocarriers at the passivation interface, it is noticed that the photocarriers are normally mobile and thus rather extended, while various recombination centres (mostly defects) at the passivation interface are quite localized, e.g., K centres with Si atoms bounded to three N atoms instead of four. FP methods are necessary for properly describing localized defects, while in most cases; only solid-state based envelope function approach has been able to describe the mobile photocarriers under device operation conditions (their photogeneration and transport under external bias). Therefore, for the recombination time calculations two approaches have been used about single particle wave functions of extended photocarriers and localized defects. One is to extract the total wave functions directly from the FP calculations from WP2. The other approach is to match the base functions used in solid-state envelope function theory and the ones in FP calculations. This is believed to be more suitable when states of wave functions extended over 10 nm are involved. We are now programming intensively the corresponding numerical codes, which will be used in the following task.

We have formulated the principal recombination processes, i.e., radiative recombination, electron-electron interaction (Auger recombination and impact ionization), and electron-phonon interaction. Model calculations based on solid-state envelope function approach have been performed for recombination processes in semiconductor quantum dots placed at various distances from the interface. Numerical results agree with relevant experimental data of quantum-dot based solar cell. We are now trying to replace the quantum dots by the real potentials of defects at the passivation interface and the extracted single-particle wave functions to calculate the recombination times of photocarriers at the passivation interface. We have further tried to have a close look at experimental indications about effects of defects at the passivation interface on solar cell performance. The first check is the lifetime of minority carriers measured using photoconductance decay.

The major results of the period were that computable expressions could be derived and used to give numerical values for the most important mechanisms of recombination processes occurring at interfaces. A highly interesting result was the prediction of a dominant radiative coupling over the non-radiative channels (electron- electron scattering and phonon coupling). An important ramification of this result is that structure-property relations can be achieved by virtue of the comparative simplicity of the radiative coupling over the other processes, motivating that also even more advanced calculations should be applied for that very purpose. There indeed seems to be a possibility to design cells optimal for anti-quenching this way.

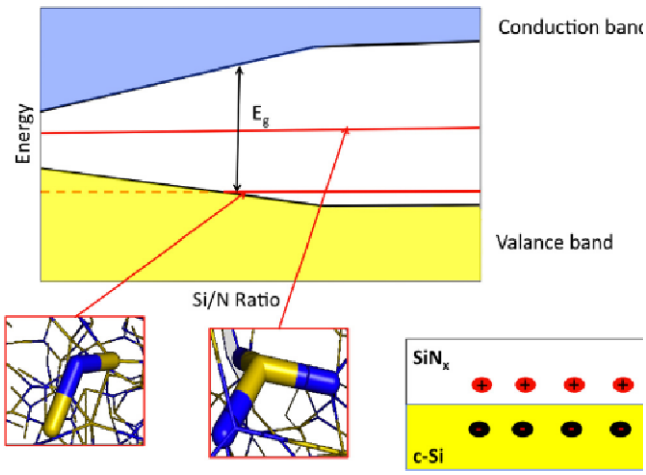

Figure 23: *(top) SiN_x band structure (schematic) as a function of the Si:N ratio. (bottom left) structure of N defect. (bottom centre) structure of K defect (bottom right) inversion layer (schematic): fixed positive charges are in the SiN_x layer* [5].

Simulations on the Si/SiN_x interface shows that the use of a graded interface significantly reduces the trapping probability by moving the recombination centres away from the crystalline silicon. This suggests that control of nitridation to produce graded interfaces can significantly improve carrier lifetimes.

Important defects along the silicon/silicon-nitride interface and in bulk silicon are predicted that have a bearing on improving the passivation quality of silicon silicon-nitride surfaces. Heavy phosphor doping or even pre-coverage of phosphorus before growing silicon nitride is predicted to improve the properties of silicon nitride interfaces significantly. The rather stable NP defect is found to most likely cause the heavily doped emitter close to the interface to be passivated upon nitridation, which can have devastating effects on the emitters.

A final major result was experimental; fluorescence measurements of devices indicate strong fluorescence peaks just below the silicon band gap. These may origin from the radiative recombination centres at the Si side of the interfaces that can access easily the photo carriers in Si bulk due to the laser excitation. Such measurements may thus eventually be used to screen various materials/device configurations for reducing radiative recombination.

WP5: Application of the modelling set to improve contacting

Recent commercial Ag-pastes are able to form contacts with emitters with significantly lower phosphorous surface-concentrations. To understand the reasons we formed contacts with four differently doped emitters with three of the most recent Ag-pastes. On the microscopic level, Ag-crystallites grown into the emitter in direct contact with the bulk of the Ag-finger play a major role in current transport. Here we find that while partially glass-free pyramid tips leading to such direct contacts are observed no matter what the level of the emitter doping, the Ag-crystallite density and depth grown into Si resulting from a specific paste mainly depend on the electronically inactive P-content in the Si emitter within the so-called dead-layer, see Fig. 24.

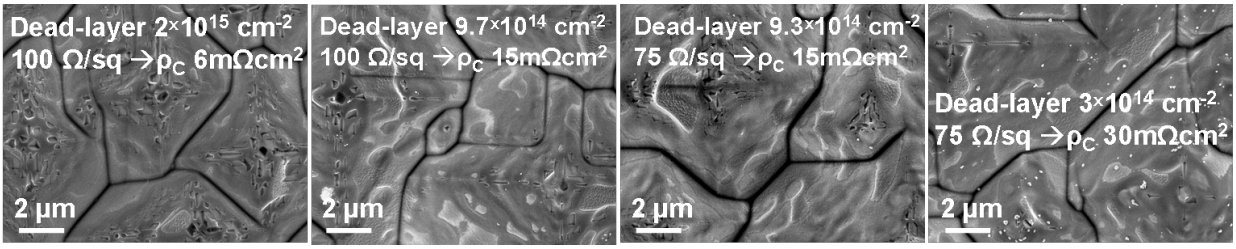

Figure 24. *SEM micrographs after full etch of the contact as resulting from the same paste on four different emitters with varying electronically inactive phosphorus-concentration (dead-layer).*

With most recent best-performing pastes the resulting Ag crystallite densities grown into Si are considerably less dependent on the dead-layer, thus good contacts can be formed to advanced emitters.

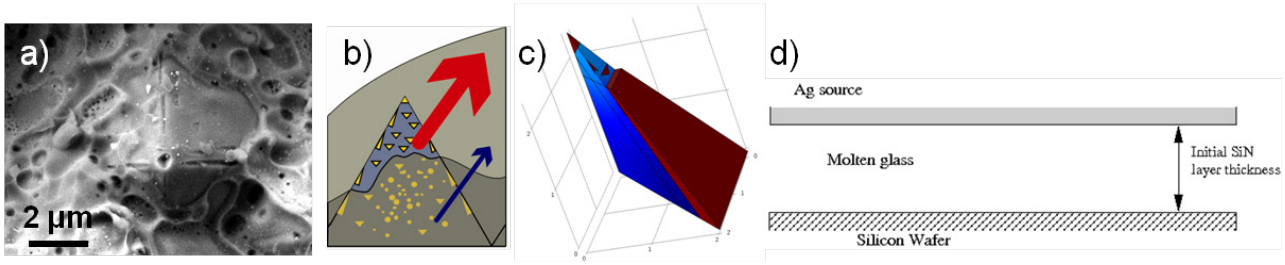

Figure 25. a) *SEM of pyramid underneath the Ag finger, featuring direct contacts.* b) *Schematic illustration of the experimentally evaluated current transport path hierarchy.* c) *Idealized geometry consisting of p-Si substrate, n-Si emitter layer, and glass partly covering the surface.* d) *Simplified model of solid silver on molten glass for silver dissolution-transport modelling.*

Based on the experimental confirmation of the existence (Fig. 25a) and importance (Fig. 25b) of direct contacts between the Ag finger and the cell surface, realistic models of the solar cell contact formation were established. The model of the conductance thus contains such direct contacts within the observed geometries (Fig. 25c) and the metallisation process model focuses on the amount of silver crystallized at the silicon surface (Fig. 25d).

Detailed mathematical models have been implemented in realistic geometries for the Ag-Si contacting interface based on Schottky barrier models for the local resistivity. An idealized geometry is generated based on detailed investigation of real contacting interfaces (textured surface) by SEM, see Fig. 25a) and c). The models allow for identification of conductivity losses related to surface fraction, orientation and shape of silver crystallites. The conductance model predictions of contact resistivity changes with varying doping type and profiles, Si etch depth, removal of glass, as well as temperature, are in agreement with our experimental data and result in deeper and more fundamental understanding of contact formation. The contact resistivity resulting from identical microscopic contact configurations on typically used higher and lower phosphorous doped solar cell emitters varies only slightly, e.g. only by a factor of two when reducing emitter doping from 60 to 80 Ω/sq within typical industrial emitter doping profiles. The experimentally observed trend of reduction of contact resistance upon reduction of temperature is found to be related to the improved conductivity of the emitter layer with lower temperature and it is accentuated by the doping profile variation. When contacting boron-doped emitters, despite the presence of some directly contacted Ag-crystallites at the pyramid tips, measured contact resistivities are two orders of magnitude higher. From modelling we conclude that despite the lower p-type Schottky barriers, also with identical microscopic contact configuration, contact resistivity would be increased by one order of magnitude because of less efficient hole transport and significantly reduced peak doping of the boron doping profile.

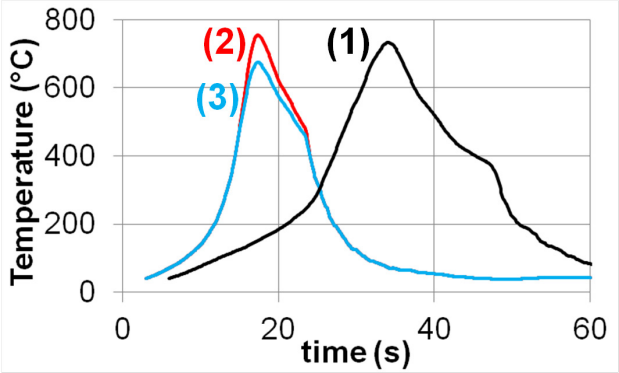

Figure 26. *Firing profiles chosen for modelling comparison.*

A mathematical dissolution-transport model was developed for solids in liquid solvents, at temperatures below the melting temperature of the solid. A thermodynamic procedure was developed to prepare input for the dissolution-transport model, enabling simplified modelling of complex liquid mixtures. This metallisation process model was employed to study the crystallization of silver at the silicon surface, see Fig. 25d), in dependence of realistic firing temperature/time profiles, and liquid layer thicknesses separating the silver body and the Si surface. The modelled trend of silver content in Si as resulting from simple experimental glass frit composition (only PbO, B_2O_3 and SiO_2) together with different experimental firing profiles is in agreement with the equivalent experimental data, see Fig. 26 and Table 4.

The use of silver in the rapidly growing solar cell industry is problematic, due to high price and eventually to availability. Replacement of silver is a very challenging task: Equally well conducting metals are like gold even more expensive, or like copper detrimental for long-term solar cell

Table 4. *Comparison of experiment with model prediction.*

	Firing temperature profile	***(1)***	***(2)***	***(3)***
exp	*EDX Ag content in Si (mass%)*	3.2	34	4.6
model	*Continuous Ag layer on Si of thickness (nm)*	1.4	2.2	1.1

performance. Because Cu, the only sufficiently conducting and cheap alternative metal cannot be put in direct contact with Si, we focused on splitting up the current Ag-based pastes bi-functionality of forming good contact to Si and simultaneously transporting the collected current in well conducting lines. Nickel builds a good contact to silicon because of Ni silicide formation and is a good Cu diffusion barrier. While Ni and Cu are equally fast diffusers in Si, Cu has a higher solubility in Si than Ni and Cu precipitates (Cu_3Si) fit worse into the Si lattice than Ni precipitates ($NiSi_2$). Therefore Ni is less detrimental for the solar cell efficiency. Also Zn could be a possible material to substitute Ag because of low cost and alike properties. Despite the large temperature/time parameter space tested, neither with Ni- nor with Zn-paste could good contact to Si be formed. The microscopic interfaces resulting from high-temperature fast-firing are identical for Ni- and Zn-paste: Pb-crystallites with small Ni respectively Zn content grow into Si, see Fig. 27a) and b). Their shapes are the same as those of the Ag-crystallites. Tempering of Ni-paste only leads to insufficient Ni silicide formation, see Fig. 27c).

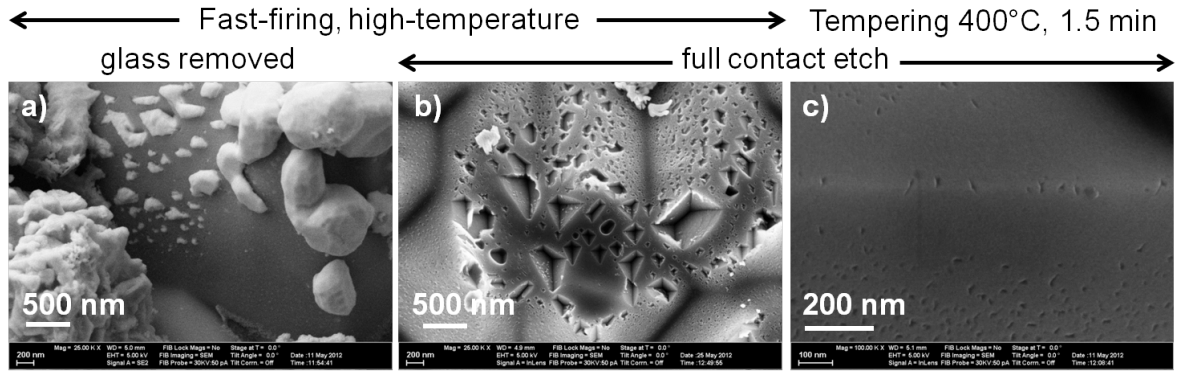

Figure 27. *SEM micrographs of the Ni paste contact composition.* a),b) *At high-temperature fast-firing Pb-crystallites with only little Ni content grow into Si.* c) *Minor Ni silicide formation is observed at lower temperature tempering.*

Instead of forming contact to Si, the tested alternative metals Ni and Zn severely reduced the solar cell efficiency by detrimental in-diffusion when used analogously to silver in a short high-temperature firing step. Screening of silver replacement materials has generally shown that it is fundamentally unlikely that contact formation can be achieved analogous to silver/glass within a short high-temperature firing step.

The understanding of the contact formation enabled Sunways to demonstrate that a contact formation process in combination with a lowly doped solar cell emitter is implementable in an industrial process.

WP6: Application of the modelling set to improve passivation

The work carried out in this workpackage contains four main topics:

1. Research and development of improved passivating layers based on SiN_x:H

2. Research and development alternative layers for passivation
3. Application of improved passivating layers in an industrial environment
4. Relate the modelling results to the experimental ones.

There was a close cooperation between the partners that performed the experimental work and the partners that carried out the modelling and theoretical part of the project.

The main results of this workpackage have been published or will be published later this year.

Research and development of improved passivating layers based on SiN_x:H

In the first part of the project different characterization techniques were evaluated within workpackages 1 and 4. High resolution Transmission Electron Microscopy (TEM), Fourier Transform InfraRed (FTIR) spectroscopy, X-ray Photoelectron Spectroscopy (XPS), spectroscopic ellipsometry and Time of Flight Secondary Ion Mass Spectroscopy (SIMS) were used for detailed characterization of the layers. In the second part of the project the physical properties of the layers were related to passivating properties. The passivating properties were measured by Quasi Steady State Photoconductance (QSSPC) and Capacitance-Voltage Metal-Insulator-Semiconductor (CV MIS) measurements. With the first method the effective lifetime of the minority charge carriers can be determined. From this lifetime the effective surface recombination velocity S_{eff} can be calculated. With the latter the density of states at the interface D_{it} and the number of fixed charges in the layers (Q_f) can be determined. D_{it} is a measure for the so-called chemical passivation and Q_f is the one for the so-called field effect passivation. Both D_{it} and Q_f determine the overall passivating quality. The number of fixed charges Q_f can be related to defects in the SiN_x:H layer (for example the so-called K and N centres).

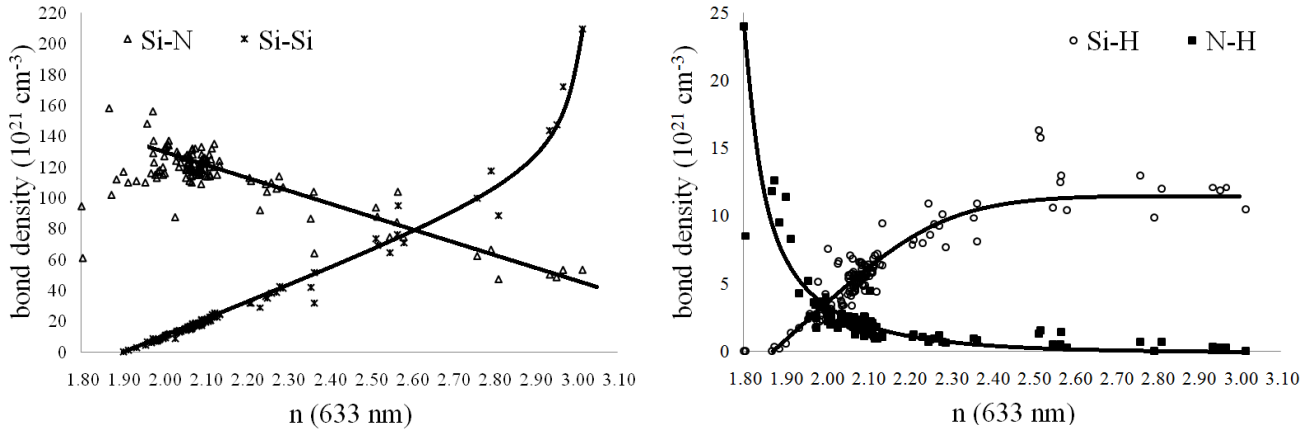

Figure 28. *A (left): Si-N and Si-Si bond densities versus refractive index n for a SiN_x:H layers with different composition. B (right): Si-H and N-H bond densities versus refractive index n for a SiN_x:H layers with different composition.*

Two examples in which the different bond densities versus the refractive index can be seen in Fig. 28A and B. It can be seen that the Si-Si and Si-H bond densities increases with n. For the Si-N and N-H bond density there is a decrease with increasing n. This corresponds to the general trends observed by others.

The FTIR spectra were analyzed in more detail and the results can be found in Fig. 29. The same peaks as shown in Fig. 28 can be found, but also the area bond density of the Si-N peak at 790 cm^{-1}. This peak represents the bonds with a locally distorted configuration. This distortion could be related to defects in the SiN_x:H layer, and thus Q_f. In Fig. 30 plots of Q_f and D_{it} versus n are shown. It is clearly visible that Q_f can be related to the distorted Si-N configuration, which is confirmed by

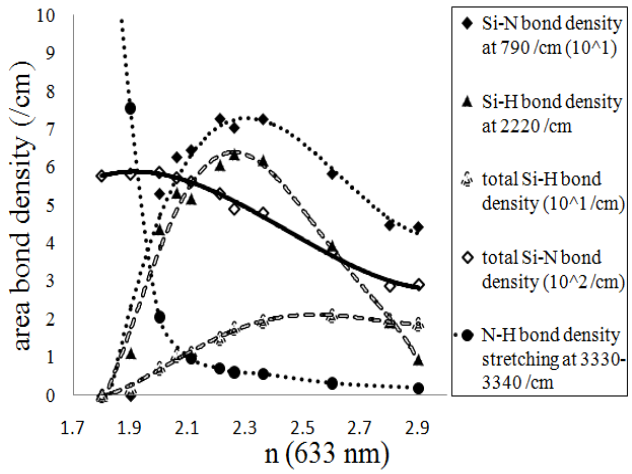

Fig. 29 *Relationship between (the peak areas of) the Si-H bond density, the deconvoluted Si-H bond density at 2220 cm^{-1}, the Si-N bond density, the deconvoluted Si-N bond density at 790 cm^{-1} (distorted), N-H bond density and n.*

Molecular Dynamics (MD, see WP4). Furthermore it can be seen that D_{it} and Q_f follow the same trend (the higher Q_f, the higher D_{it}). For solar cell applications the effect of D_{it} and Q_f are competing with each other. Lower D_{it} will result in better chemical passivation, while a lower Q_f will result in reduced field effect passivation. Good passivation is found for n values above 2.1. However, for the higher n values absorption in the SiN_x:H layers becomes limiting, and those layers cannot be applied to solar cells (it will result in lower efficiencies).

Based on this information we have improved the passivating quality by using layers with a gradient in composition (and therefore n). At the Si-SiN_x:H interface the layer is more Si rich (higher n) and at the interface with air the layer is more N rich. On completed solar cells a clear improvement in blue response was observed which resulted in an efficiency gain of about 0.2% absolute.

More details can be found in M.W.P.E. Lamers, K.T. Bulter, P.E. Vullum, J.H. Harding, A.W. Weeber, "Characterization of a-SiN_x:H layer: Bulk properties, interface with Si and solar cell efficiency", accepted by *Physica Status Solidi A,* (2012).

Research and development alternative layers for passivation.

Surface passsivating properties can be changed by varying D_{it} and/or Q_f. We aimed to increase Q_f for SiN_x:H layers for layers with lower n, and thus lower absorption, combined with good bulk passivation. In our case we applied (homogeneous) SiN_x;H layers with n below 2.1 and before the actual deposition an NH_3 plasma pre-treatment was carried out. With this pre-plasma Q_f could be increased to much higher values, and thus to improved surface passivating properties. In Fig. 28 the effect of the pre-treatments on Q_f and D_{it} can be found and the effect on surface passivating quality for p-type and n-type surfaces. Q_f and D_{it} can be varied by changing the temperature of the pre-treatment. The higher the temperature the more nitrogen will be introduced in the Si lattice resulting in more defects, and thus higher Q_f. This was confirmed by MD (see WP4).

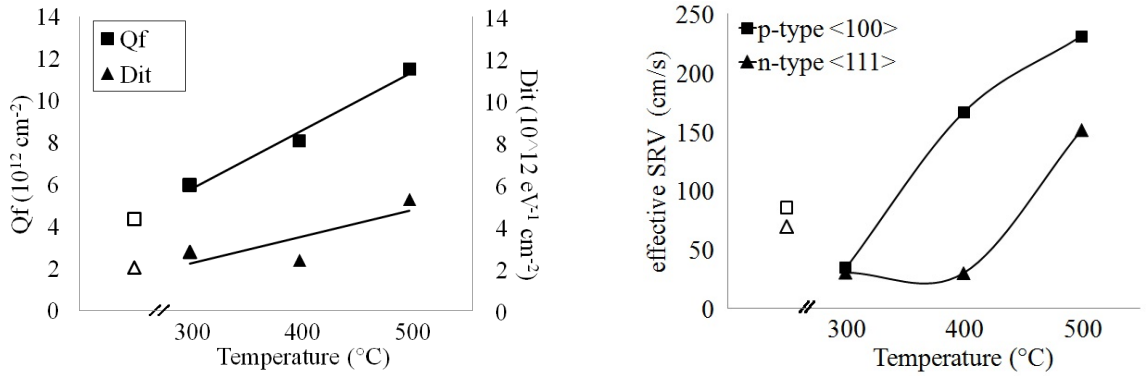

Fig. 30. *A (left): Effect of the NH_3 plasma pre-treatment on Q_f and D_{it}. B (right): The same, but then for the surface passivating quality.*

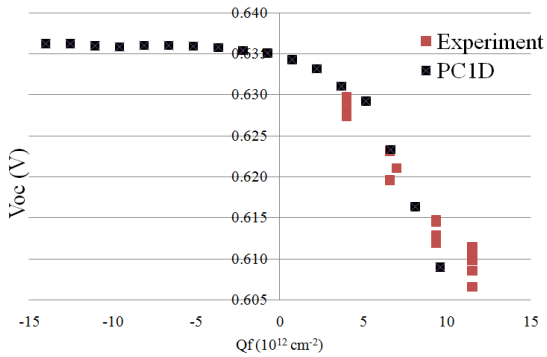

Fig 31. *V_{OC} of n-type cells as function of Q_f. Both experimental and simulated data are shown.*

The plasma pre-treatment process was evaluated on completed solar cells (both n-type and p-type). For p-type cells with an n-type emitter a slight increase in efficiency was observed. For n-type cells with a p-type emitter increasing Q_f will result in more depletion and therefore lower V_{OC} values. By carrying out a plasma pre-treatment it was possible to vary Q_f resulting in a 20 mV change in V_{OC}. Together with PC1D simulations the results can be found in Fig. 31.

More details can be found in M.W.P.E. Lamers, K.T. Butler, J.H. Harding, A.W. Weeber, "Interface properties of a-SiN_x:H/Si to improve surface passivation", Solar Energy Materials & Solar Cells **106**, 17-21 (2012). Oral presentation at SiliconPV 2012 (Leuven, Belgium).

Application of improved passivating layers in an industrial environment

SiN_x:H layers with a gradient and layers with NH_3 plasma pre-treatments were applied to solar cells processed in an industrial environment. In both cases an efficiency gain has been observed. For gradient layers the efficiency gain was about 0.3% absolute, and performing a plasma pre-treatment resulted in a gain of about 0.1% absolute. The improved passivation process will enable both Sunways and Isofoton to improve their cell manufacturing process resulting in better efficiencies.

Relate the modelling results to the experimental ones.

Experimental data of thoroughly characterized SiN_x:H layers (high resolution TEM, XPS) were used as input for MD and *ab initio* Density Functional Theory (DFT) studies. Both MD and DFT show that Q_f and D_{it} can be related to defects and distortions. With DFT it is shown that the K centers are the dominating defects resulting in higher D_{it}., which will result in higher Q_f. SiN_x:H layers with lower x will result in an increase of Q_f. These results correspond to the experimental ones. More results on DFT studies can be found in WP2.

Plasma pre-treatments can be simulated using MD. The MD simulation has shown higher defect concentrations for increased nitridation. This effect is confirmed experimentally as well.
More results on MD can be found in WP4.

More details will be presented by M.W.P.E. Lamers *et al.* during the SiliconPV 2013 in Hamelin (so-called extended oral presentation), and will be published in Solar Energy Materials & Solar Cells.

Acknowledgements

In addition to the HiperSol grant from the European 7th Framework programme (Grant No. 228513) we acknowledge the Norwegian NOTUR high-performance computing facilities and the UK's national high-performance computing service HECToR (through USFD's membership of the UK's Materials Chemistry Consortium, which is funded by EPSRC grant EP/F067496) for providing needed supercomputer resources. Significant high performance compute time was also made available on the Vienna Scientific Cluster (VSC).

4.1.4 Potential impact

HiperSol is a fundamental project with an impact covering many fields of materials science as well as improvements in processing and properties of silicon solar cells.

4.1.4.1 Scientific impact

The phrase, *the interface is the device,* first coined by Herbert Kroemer (Nobel Prize Winner for Physics, 2000), is becoming increasing true as nanotechnology advances. However, if the interface is to become the device, then understanding at the atomic scale is essential. Moreover, this nanoscale understanding must then be linked to the other relevant length-scales in the system. The enduring necessity of using models with classical force-fields arises from two factors: modelling an interface requires a large number of atoms and it is always necessary to model a range of interfaces to understand a system. This work demonstrates that it is possible to generate suitable force-fields and use them to construct models of complex hetero-interfaces that can be linked to experiment and device performance. The strategies and methodologies developed here have much wider application than to the specific case of solar cells. For example, the rapidly growing field of adaptive oxide electronics requires the understanding of charge transport mechanisms, particularly at interfaces between interconnects and devices where band alignment influences whether Schottky barriers or ohmic contacts form.

As electronic devices shrink in size, scattering at defects and interfaces plays an increasing role and an atomistic description becomes important, maybe even mandatory. Hence, classical electronic device simulations, which are nowadays usually based on Boltzmann's transport equation, will ultimately be replaced by simulations that take into account the one-electron Schrödinger equation (treating non-interacting electrons) with a suitably parameterized weak interaction between electrons and interactions between the electrons and the lattice.

On the other hand, ab-initio (parameter-free) methods are available aiming to solve the true many electron Schrödinger equation (treating strongly interacting electrons). But the solution of the many electron Schrödinger equation is only possible for very small systems.

Our efforts contribute to the merger between classical electronic device simulation (aimed at macroscopic models containing billion of atoms) and full ab-initio simulations (aimed at few atoms). It aims to bridge this gap addressing systems and models containing typically 100.000 atoms. If we achieve our ambitious goal, we can enduringly change the methods used to simulate electronic devices. This might yield new insight in solar cells, but the methods developed here are broadly applicable to other electronic devices and nanostructures.

In addition, the methodological development on the ab-initio side of the aforementioned merger is of obvious benefit to the field of ab-initio modelling *per se*. For instance, the advanced iterative matrix diagonalisation techniques implemented to solve inner eigenvalue problems, and the algorithms to efficiently evaluate Auger recombination rates from ab-inito one-electron orbitals will be useful in many applications far beyond the scope of the HiperSol project.

The HiperSol network has offered new understanding as well as new algorithms for how to reach that understanding of the major recombination events. Thus the operation for the device is not only dependent on how it is activated but also how it can avoid losses to various deactivation processes. Recombination means quenching of the holes and particles (or electrons) that ideally should remain separated through the interfaces and through the crucial parts of the device. Thus HiperSol has put forward "structure-property" relationships on how to accomplish an "antiquenching design" in order

to limit such recombination (or quenching) to a minimum. It has addressed all three major channels of such recombination, namely radiative recombination (where the hole particle excitation, or exciton, is recombined though spontaneous emission of a photon; phonon quenching (where electronic excited and ground levels "connect" to each other by the vibrational or lattice degrees of freedom of motion); and finally, non-radiative electronic coupling (sometimes called Auger coupling, which is a complicated local, but often very effective, process for the decay of the excitations if this this path at all is energetically possible).

One major achievement of HiperSol it that it has been able to address all these three decay mechanisms in one formulation, another achievement is that it could associate numerical values to the formulation under certain assumptions or parameterization relevant for the real device situation. Through HiperSol we could thus put numbers on these processes and could relate those numbers rather closely to the design of the device in terms of materials and geometrical configuration. The understanding this gives, and will give through further extensive application of the derived formulas is a strategic accomplishment of the network which can give future impact, improvement and possible breakthrough in this important technology area.

4.1.4.2 Impact on PV

The insight acquired through the modelling activities can have valuable impact on the choice of future metallization schemes. The results have confirmed our hypothesis that metal transport through glass may be a rate limiting step in the contact formation, and this can be of important assistance when developing improved schemes for screen printing excluding the use of Pb or other unwanted elements in the paste. Also, the microscopic understanding of the electrical conductivity through various interfaces between Ag and Si can have significant impact on future metallization technologies, both those utilizing screen printing and other methods.

The PV industry has developed very fast in recent years in terms of market size and of reduction of cost per watts for the complete PV-system. It is expected that the growth of PV will continue for the next year and the search for implementing new technologies to reduce cost and to increase system efficiency will intensify. The main focus will lie on the replacement of the screen printed aluminium on the rear side of the solar cell for surface passivation by a dielectric layer and the reduction or even replacement of the use of silver for the contact formation. The assessment of these technologies requires a deep understanding of the underlying physical properties. As the project contributed a lot in the understanding passivation metallisation the results have the potential to help decision takers in PV-industry to decide for the investment in the appropriate technology.

At the industry-scale experiments at Isofoton on shallow low-doped emitters based on results from WP5, an improvement in the efficiency could be shown, essentially due to the reduction in superficial recombination, above all in the emitter. With these new cells, the efficiency over the current cells is increased by a factor of 3.6%, with the process intervals being sufficiently large, which we consider to be an important result.

For future high-efficiency cell concepts excellent surface passivation will be more important. Within the HiperSol project surface passivation of SiN_x;H layers have been extensively researched (both experimental and theoretical) and resulted in a better understanding. This knowledge can be applied to other new passivating layers and even passivating contacts that will be applied to future high-efficiency cell concepts.

4.1.4.3 Dissemination activities and exploitation

The dissemination activities for WP1 were publications in the academic literature and conference presentations. Exploitation is in conjunction with other work packages that used results from this one and is discussed below. At the university of Sheffield, a postdoc (Keith Butler) was funded by the HiperSol project and has applied a range of simulation methods to problems in photovoltaics. He will continue to work in this area. An MSc student (Tong Long) also did his project in the area of interfaces in solar cells.

As for WP1, the dissemination activities for WP2 were mainly publication in the peer-reviewed academic literature, and several presentations at international conferences. In addition, an appreciably part of the work at University of Vienna was performed by the PhD-student Leif-Eric Hintzsche, who will defend his thesis at the beginning of 2014. Furthermore, all algorithmic development within WP2 has been absorbed into the Vienna Ab-initio Simulation Package (VASP). VASP is a very prominent software package within the computational materials science community, with more than 2000 license holders world-wide. As such, the progress and algorithmic developments on the ab-initio side of WP2 of the HiperSol project will be directly available to a large and diverse part of the computational materials science community.

SINTEF educated two master students in WP3; Dan Michael Olsen Heggø and Astrid Marie Flattum Muggerud. They have achieved a broad overview of solar cell technology in addition to detailed scientific competence within DFT calculations and TEM characterization. Also, Espen Flage-Larsen worked as a postdoc at SINTEF, funded by the HiperSol project. He is now permanently employed in SINTEF, and is attached to several new and relevant projects.

At ECN internships of one bachelor student (Bart Teussink from Fontys University of Applied Sciences) and one master (Le Thang Nam from the Technical University of Munich and Nanyang Technological University) student were carried out. Le Thang Nam performed detailed characterization on passivating layers using FTIR, Kelvin Probe measurements, CV MIS and Spectroscopic Ellipsometry. Bart Teussink carried out process optimization on different passivating layers applied by PECVD (silicon oxide, silicon nitride, stack layers, etc.). With these studies more fundamental knowledge on the physical properties of the layers with respect to the passivating quality was gained. PhD student Machteld Lamers will finish her PhD thesis in 2013. The main part of her thesis, which will be made available in the public domain, will contain R&D results obtained in the HiperSol project. Several papers (a large part of these papers were written together with partners) have been published already. Together with industry partners Sunways and Isofoton improved processes that were developed based on the HiperSol results were evaluated and an efficiency gain was observed. ECN will use (or actually is already using) these improved processes in its baseline processing, and also in future processing schemes for high efficiency solar cells.

At ISC Konstanz the PhD-student Enrique Cabrera was recruited for the HiperSol project, generating a new doctorate, with a thesis submitted in the field of solar cell metallisation. This scientist is a valuable project contribution for both scientific fields in need of highly educated and trained researchers and for an industry sector in a process of rapid growth. His thesis produced in the HiperSol project will be made available in the public domain.

Sunways worked closely together with ISC and ECN in preparing and analysing samples from industrial processes. Therefore Sunways gained a more fundamental understanding of their actual industrial process and also of possible future processes.

During the time of the project Sunways could decrease the production costs of solar cell by more than 5% only by improving cell efficiency. The results of the project made an important contribution to this improvement.

Isofoton have worked closely together with ISC and ECN in preparing and analyzing samples from industrial processes. Nitridation process for passivation improvement has been investigated, and the contacting for low resistivity emitter has been improved. Isofoton industrial solar cell efficiency has increased about 5.7% from HiperSol project beginning and the manufacturing cost has been reduced about 5.4%.

Dissemination of the network results have occurred through user contact, conferences and through normal academic channels. At KTH HiperSol results have been ventilated and discussed in the forum of the recently inaugurated research centre JINGLE - Joint institute of Nanotechnology for Global Energy, where Hans Ågren is director, and during the kick-off meeting of that centre in May 3-5, 2012, where a session dedicated to solar energy was included. Network results and the network as such have also been connected to or discussed with respect to other energy initiatives at KTH, n.b.

- The KTH Platform for energy research.
- The common KTH – UU energy consortium STANDUP, funded by the government strategic initiative, and with Escience aspects to eSSENCE and SeRC, the two strategic e-science initiatives in Sweden.
- The KTH platform and STANDUP connect to solar cell constellations in EIT energy, the European Institute of Technology. Here HiperSol has played a non-negligible role.
- The HiperSol work has been conducted in line with the KTH policy of strengthened international collaboration, as exemplified by the agreement between KTH and the China Scholarship Council for student and researcher exchange, in which energy research has a central role. A Chinese senior as well as a PhD student has been enrolled in HiperSol as results of this exchange.

4.1.5 Project data

The HiperSol project has an open website available on http://www.sintef.no/Projectweb/HiperSol/ and http://cordis.europa.eu/projects/rcn/92605_en.html. On these, information about the project vision, goals, consortium publications and events are published. The coordinating organisation was SINTEF, and the coordinator was Jesper Friis (jesper.friis@sintef.no, +47-98230458). The logo of the project is shown below.

HiperSol consortium

The HiperSol project was executed by 8 partners from 7 European countries. The involved organisations are listed below:

Research institutes

Stiftelsen SINTEF, Norway
Contact person: Jesper Friis
E-mail: jesper.friis@sintef.no

Stichting Energieonderzek Centrum Nederland (ECN), The Netherlands
Contact person: Arthur Weeber
E-mail: weeber@ecn.nl

International Solar Energy Researchcenter Konstanz (ISC), Germany
Contact person: Sara Olibet
E-mail: sara.olibet@isc-konstanz.de

Industrial partners

Sunways Aktiengesellschaft, Germany
Contact person: Daniel Reinke
E-mail: daniel.reinke@sunways.de

Isofoton, Spain
Contact person: Miguel Ángel Vázquez
E-mail: m.vazquez@isofoton.com

Universities

Universität Wien, Austria
Contact person: Georg Kresse
E-mail: georg.kresse@univie.ac.at

The University of Sheffield
Contact person: John Harding
E-mail: j.harding@sheffield.ac.uk

KTH (Kungliga Tekniska Högskolan), Sweden

Contact person: Hans Ågren
E-mail: hagren@kth.se